DOPPLER-FREE SPECTROSCOPY OF ACETYLENE IN NEAR INFRARED SPECTRAL REGION INSIDE PHOTONIC BAND GAP FIBER

By

Rajesh Thapa

B.S., Tribhuvan University, Nepal, 1995
M.S., Tribhuvan University, Nepal, 1998

A REPORT

submitted in partial fulfillment of the

requirements for the degree

MASTER OF SCIENCE

Department of Physics

College of Arts and Sciences

KANSAS STATE UNIVERSITY

Manhattan, Kansas

2005

Approved by:

Major Professor

Kristan Corwin

ABSTRACT

We investigate the nonlinear spectroscopy of acetylene in the near infrared region inside a photonic band gap fiber. The near infrared region of the optical spectrum is an area of intensive research due to its relevance to telecommunication and optical metrology. Acetylene provides a large number of reference transitions coincident with the international telecommunication band. Acetylene contains about 50 strong lines between 1510 nm and 1540 nm in the $\nu_1+\nu_3$ ro-vibrational combination band. We have observed the Doppler-free saturated spectrum of several of these lines. The light from a tunable diode laser at ~1531 nm, resonant with the P(11) transition, is amplified by an erbium doped fiber amplifier and split into a strong pump beam and weak probe beam which counter-propagate inside the gas-filled fiber. The measured Doppler linewidth of the P(11) line at room temperature is about 467 MHz wide. The sub-Doppler profile over a pressure range of 200-1600 mT appears as a narrow absorption feature about 20-40 MHz wide, even at the low pump power of ~10 mW. It is found that for a fiber with an 80 cm length, $20\,\mu m$ core size, pumped with 29 mw, the optimum pressure is ~530mT. But the optimum pressure condition will further decrease when the fiber length increases.

Chapter	Table of Contents	Page

LIST OF FIGURES

Acknowledgement

I would like to express my sincere gratitude to my advisor Professor Kristan Corwin for her continuous guidance, encouragement and timely comments throughout the course of this work. I extend thanks to my committee members Professors C. Lewis Cocke and Brett D. DePaola for their valuable comments and suggestions concerning the contents of this work. I am also thankful to Prof. Larry Weaver for his guidance during my coursework and research. I would also like to thank Prof. Brian Washburn and Dr. Ahmer Naweed whose suggestions have always been valuable. I am very grateful to Prof. Dean Zollman who was very supportive when I needed help. My thanks to Jane Peterson and Peggy Matthews who were very helpful with office work. Big thanks to all the professors whose courses I took.

I would like to thank Mohammad Faheem whose lab setup I used at the beginning. My thanks also goes to my colleague, Kevin Knabe, who was especially helpful during analysis and fitting of the data. I would like to thank all the undergraduates who have worked in the lab. A big thanks to the JRM family, especially, Mike wells, Scott Chainey and Michael James for their assistance in various phases of this work.

To my parents and grandmother goes a very special thanks. Their love and encouragement has given me strength and support. Many thanks to my wife, Sunita, who always supported in various ups and down in my life and to my little son, Samyak, who is the major source of inspiration to succeed in life.

CHAPTER 1

Introduction

Laser spectroscopy has its greatest impact on the present state of atomic and molecular physics. It has led to advances in the precision with which spectral line frequencies can be measured. This precision has been obtained by counter-propagating two laser beams through an absorption sample. This is also called a Doppler-free technique [1] because only the molecules that have zero velocity along the axis of beam propagation see both the pump and probe beam and give rise to the narrow absorption feature.

Optical communication technologies rapidly evolved during the 80's, several related devices such as semiconductor lasers, modulators, and detectors were developed to operate in near infrared region (~1.54 μm wavelength). Much work has been done to measure the frequency of weak molecular band transitions in the near infrared region[2-7]. We are developing a frequency comb generated with a chromium-doped forsterite femtosecond laser to measure the frequency of the signal of our interest[8]. There are several overtone and combination bands of acetylene in the infrared region but the v_1+v_3 combination band has a relatively strong absorption feature. Furthermore, its spectrum overlaps the C-band very well. Acetylene spectra offer many well-separated transitions (Fig.1) and lack a permanent dipole moment which makes it relatively immune to external fields and shifts. Precise realizations of these lines have so far relied on saturation spectroscopy performed with a power build up cavity. Acetylene has been considered as a basis of international frequency references in near IR region with accuracies in the kHz range [9-11]. Even though these cavity-based references are

relatively accurate, they are not readily portable. Photonic band gap (PBG) fibers offer an excellent medium in which to perform spectroscopy on weak molecular transitions to combine both the portability and accuracy of the frequency references in optical metrology. We expect to develop a portable frequency standard to achieve a target uncertainty of less than 1 MHz using PBG fiber.
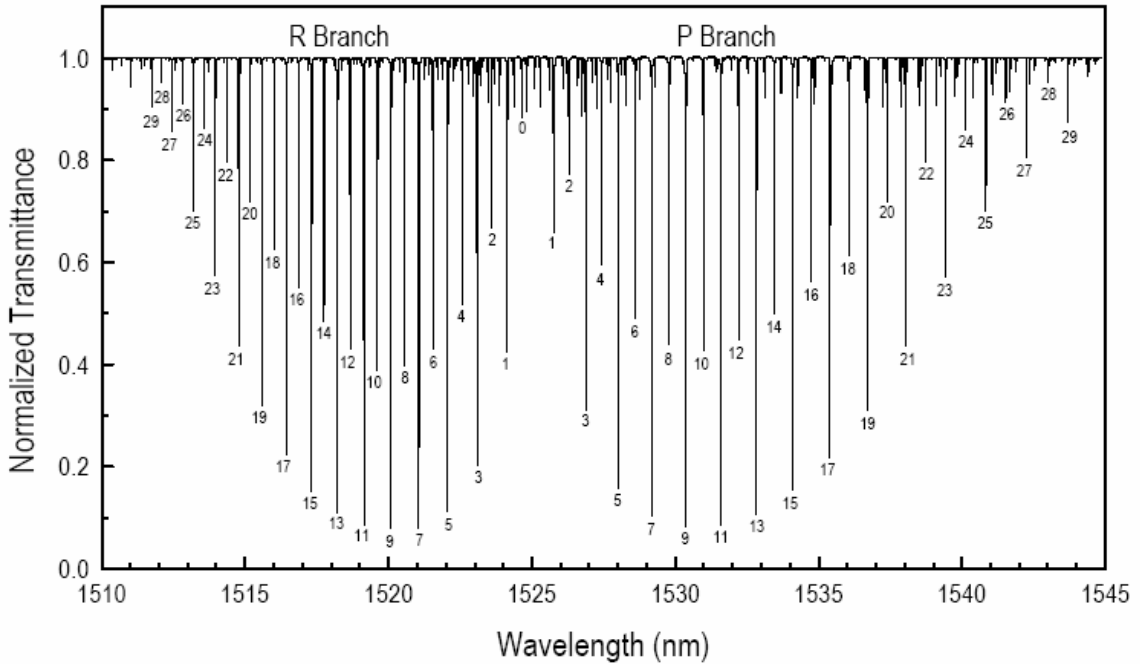
Fig. 1.1. *spectrum of v_1+v_3 combination band of acetylene[4].*

These fibers rely on a regular microstructure incorporated into their cladding which drastically alters its optical properties and delivers significantly improved performance over an ordinary hollow core fiber, as shown in Fig. 2 [12]. Guiding of light through these PBG hollow core fibers is not due to total internal reflection of light but due to existence of the PBG in the transmission spectrum of the fiber cladding. Fibers of this type support single mode wave guiding over a remarkably broad spectral range, allowing radiation energy losses to be considerably reduced in the single mode regime

2

[13]. These fibers have been used in many application such as gas sensing [14] and wavelength conversion via rotational Raman scattering [15].
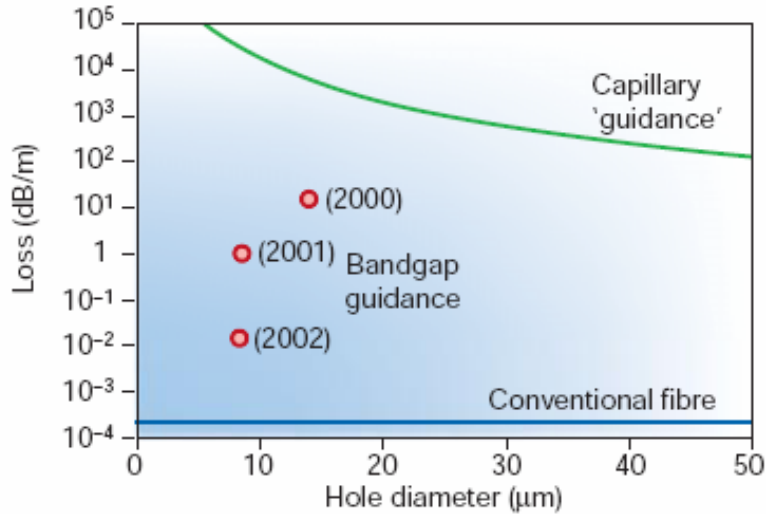
Fig. 1.2. Predicted loss from the fundamental mode in ordinary hollow core fiber and PBG fiber [12]. (Figure from Ref. [12] reproduced)

Frequency standard can also be made inside a power build up cavity. A typical power build up cavity used for saturation spectroscopy is shown in Fig. 3 [5]. A power build up cavity is an arrangement of optical components which allows a beam of light to bounce back and forth between two end mirrors to build up power inside it. The most important differences between a fiber-based standard and a build-up cavity are the proximity of the fiber surfaces to the molecules being probed, and the small beam size inside the fiber ($\sim$20 μm) as compared to cavities (500 μm). The small beam size results in short interaction time between the molecules and the laser field which gives rise to a transit-time broadening [1] of $\sim$19 MHz in a 20 μm fiber at room temperature, discussed in detail in chapter 3. The narrower lines in acetylene will require a reduction in this

transit time, either by increasing the fiber core size or by preserving coherence between the molecules and the laser field as the molecules bounce off the wall.
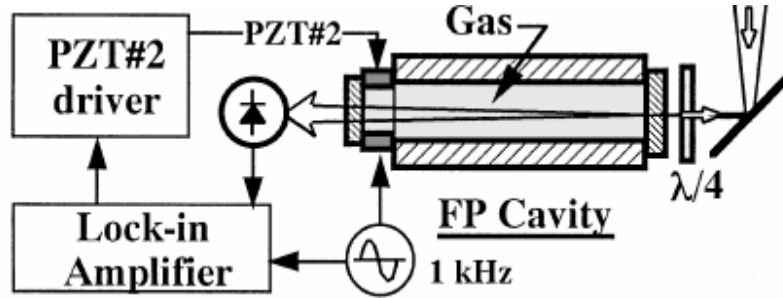
Fig. 1.3. Power build up cavity: basis for highest-accuracy measurements[5].

In this report, we present the first result of saturation spectroscopy inside hollow photonic band gap fiber. First, the theory of laser spectroscopy is reviewed, with attention paid to the origin of the broadening mechanisms. The width due to different broadening mechanisms has also been calculated. We have then explained molecular spectroscopy of acetylene with special attention given to the overtone band of the acetylene. In chapter 4, we describe briefly photonic band gap fiber and compare it with hollow capillary tubing. Chapter 5 and 6 deal in detail with the experimental set up and data analysis. In the data analysis, we have basically discussed pressure and power broadening of the sub Doppler profile of P(11) and P(13) lines. The sub-Doppler profile appears as a narrow absorption feature about 20-40 MHz wide, even at the low pump power of ~10 mW. We also figured out the optimum pressure to work with acetylene in order to get larger signal size with better signal-to-noise ratio. The report concludes with future prospects for the photonic band gap fiber as an excellent medium in which to perform spectroscopy to combine both the portability and accuracy of the frequency references in optical metrology.

CHAPTER 2

Theoretical Background

2.1. Laser Spectroscopy and various broadening mechanisms.

Laser spectroscopy has led to advances in the precision with which spectral line frequencies can be measured. The spectral resolution of all methods in gases at lower pressure in principle is limited by the Doppler broadening. At higher pressure, collision-induced broadening, called pressure broadening, is dominant. Large light intensities create power or saturation broadening. Short interaction times between the molecule and laser field give rise to transit-time broadening. Transit time broadening could be the dominant factor in Doppler-free saturation spectroscopy for small core size fiber. At sufficiently low pressures and small laser intensities, pressure broadening and saturation broadening may be neglected and the homogeneous linewidth approaches the natural linewidth, provided that the interaction of the molecules with the radiation field is longer than the spontaneous lifetime. We can minimize power broadening by working well below the saturation intensity of the molecule. Working at lower pressure minimizes pressure broadening.

2. 2. Basic Concept.

In this report, we narrow the scope of saturation spectroscopy to deal with "two level" systems as shown in Fig. 2.1. Let E_1 and E_2 be the lower and upper energy levels respectively, with population in each level denoted by N_1 and N_2 respectively. γ_1 and γ_2 are the decay rates for levels 1 and 2.
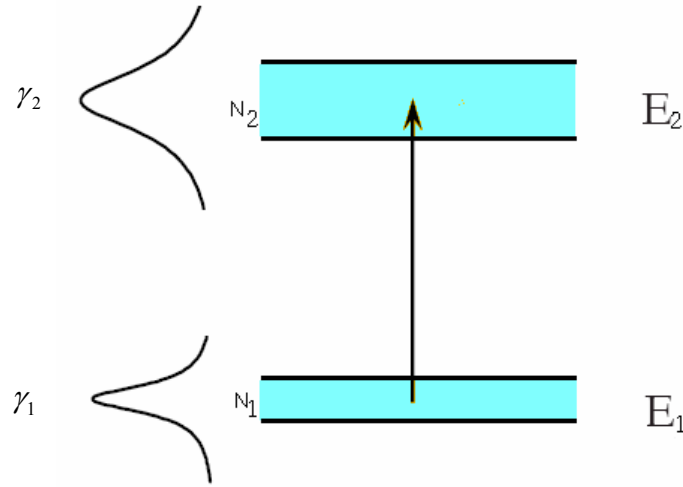
Fig. 2.1. Uncertainty in the energy level.

When a monochromatic laser beam $E = E_0 cos(\omega t - kz)$ passes through the sample of molecules, the intensity, I, of the laser beam changes according to Beer's law as

$$\frac{dI}{dz} = -\alpha I \qquad [7]$$

where $\alpha = \alpha(v)$ is the frequency-dependent absorption coefficient. The absorption coefficient $\alpha(v)$ for a transition $|1\rangle \rightarrow |2\rangle$ depends upon the population densities of the lower and upper levels, and on the optical absorption cross-section σ_{12} of each absorbing atom.

To a good approximation, for a single weak beam, $\alpha(v)$ does not depend upon position. Therefore, the overall transmission through the fiber cell of length, l, is given by

$$I = I_0 \exp[-\alpha(v)l] \qquad [8]$$

where $\alpha(v)l$ is also called optical depth.
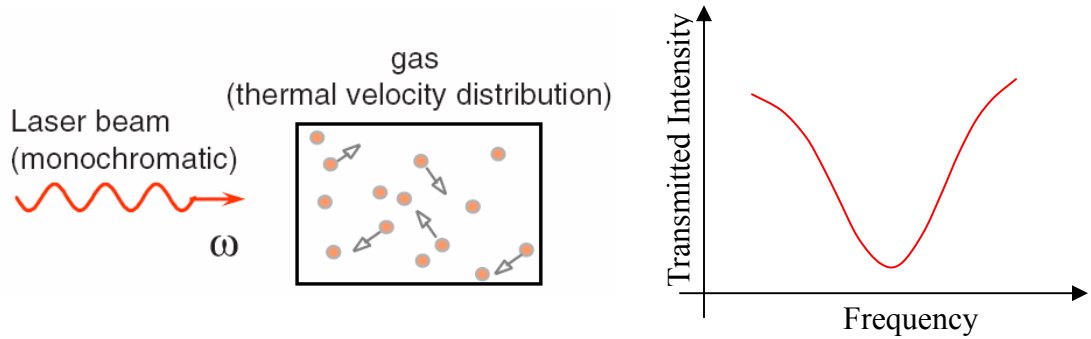
Fig. 2.2. Intensity profile due to absorption of radiation.

The exact form of $\alpha(\nu)$ depends upon physical situation. Ideally, it would be Lorentzian with a characteristic linewidth equal to that of natural linewidth of the transition (Fig.2.2). However, many mechanism such as Doppler broadening, transit time broadening, power broadening etc. serves to broaden that linewidth.

2.3. Doppler Broadening.

Doppler broadening arises from the distribution of absorption (or emission) frequencies of molecules. The distribution of frequencies occurs because the molecules have a distribution of velocities relative to the laser beam and are therefore Doppler-shifted. If we choose the z-direction to coincide with the light propagation, we can write $\omega = \omega_0 - k_z v_z$ for red-shifted radiation and $\omega = \omega_0 + k_z v_z$ for blue-shifted radiation as shown in Fig. 2.4, where v_z is the velocity of the individual molecules with respect to the direction of light propagation.

Therefore, the Doppler shift in angular frequency,

$$\omega - \omega_0 = k_z v_z = \frac{\omega_0 v_z}{c} . \qquad [1]$$
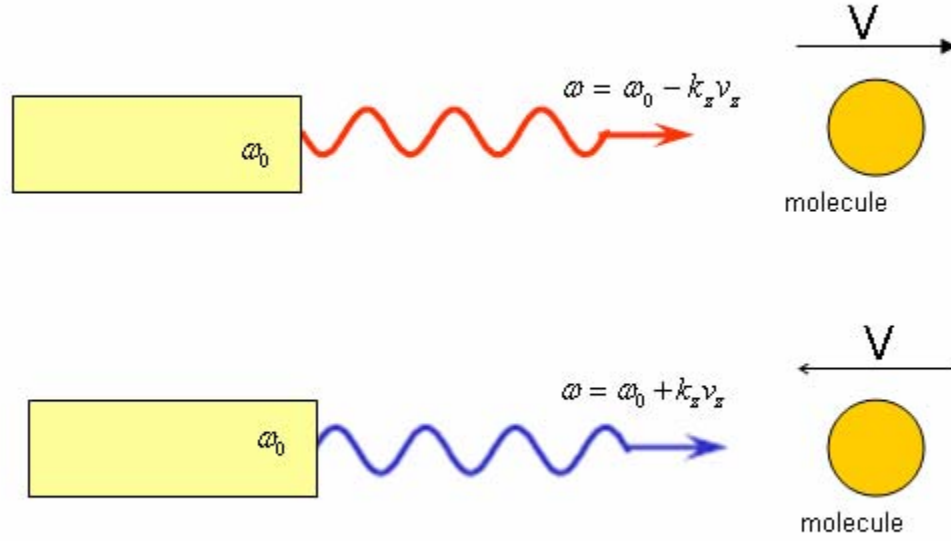
Fig. 2.3. Doppler Shift.

This clearly suggests that each individual molecule has a specific velocity and therefore contributes to a specific value of $\delta\omega_D(=\omega-\omega_0)$. Thus the value of $\delta\omega_D$ corresponds exactly to the spread of v_z.

At thermal equilibrium, the molecules of a gas follow a Maxwellian velocity distribution. Therefore the number of molecules with velocity v_z in the direction of the observed light is given by,

$$n(v_z)dv_z = N\sqrt{\frac{m}{2\pi kT}}\exp\left[\frac{-mv_z^2}{2kT}\right]dv_z \; ,$$
[2]

where N is total number of molecules and m is the atomic mass.

Substituting the expression for v_z in terms of Eq. 1 gives the number of molecules with absorption frequency shifted from ω_0 into the interval ω to $d\omega$,

$$n(\omega)d\omega = N\sqrt{\frac{m}{2\pi kT}}\exp\left[\frac{-mc^2(\omega-\omega_0)^2}{2kT\omega_0^2}\right]d\omega$$
[3]

8

The intensity of transmitted radiation is proportional to the density $n(\omega)d\omega$ of molecules absorbing in the interval $d\omega$, (Fig. 2.5)

$$I(\omega) = I_0 \exp\left[-\left\{\frac{c(\omega - \omega_0)}{\omega_0 v_P}\right\}^2\right] \qquad [4]$$

where $v_p = \sqrt{\frac{2KT}{m}}$ is the most probable velocity and m is the mass of the molecule.

This is the Gaussian profile with FWHM

$$\delta\omega_D = 2\sqrt{\ln 2}\,\omega_0\,\frac{v_P}{c} \qquad [5]$$
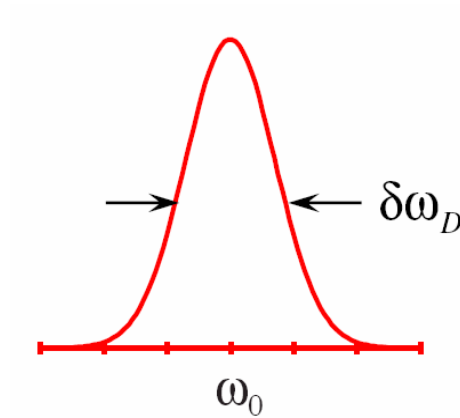
Fig. 2.4. Gaussian Lineshape.

Therefore, the line shape for Doppler broadening has the same form as the velocity distribution.

In terms of frequency units,

$$\delta v_D = \frac{2v_0}{c} v_p \sqrt{\ln 2}$$

More conveniently, we can write

$$\delta v_D = 7.16 \times 10^{-7} \times \frac{c}{\lambda_0}\sqrt{\frac{T}{M}} \quad (s^{-1}) \qquad [6]$$

9

For $^{12}C_2H_2$, M = 26.016, mass of a mole of acetylene and T $\sim 295^0 K$, temp inside lab, we get $\delta v_D \sim$ 472 MHz, full width at half maximum amplitude (FWHM), for Doppler broadened P(11) line of $^{12}C_2H_2$ at 295K which agrees very well with the experimentally observed width (Fig. 2.6).
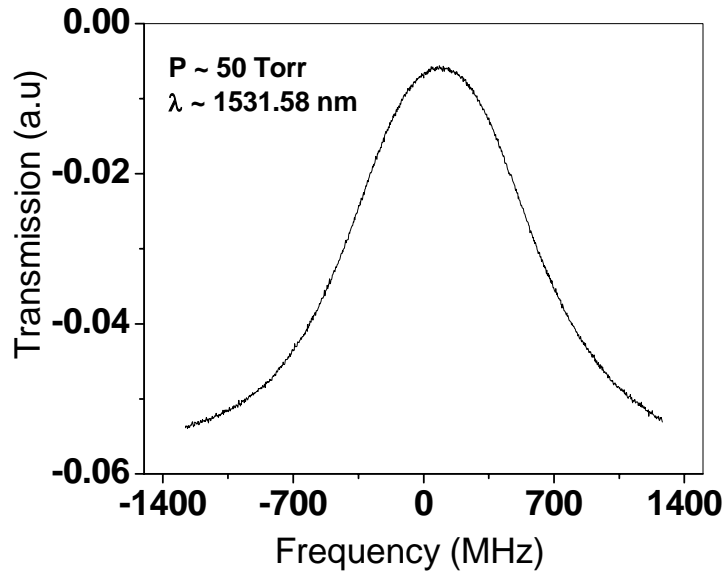
Fig. 2.5. Experimentally observed Doppler limited line shape.

More detailed consideration shows that a Doppler-broadened spectral line cannot be strictly represented by a pure Gaussian profile. The frequency response of the molecules due to their finite lifetime is represented by a Lorentzian profile. Moreover, molecules with a definite velocity component emit or absorb radiation over the range of frequencies set by the homogeneous linewidth. In fact, the intensity profile is a convolution of a Lorentzian and a Gaussian profile which is also called a Voigt profile (Fig. 2.7).

10
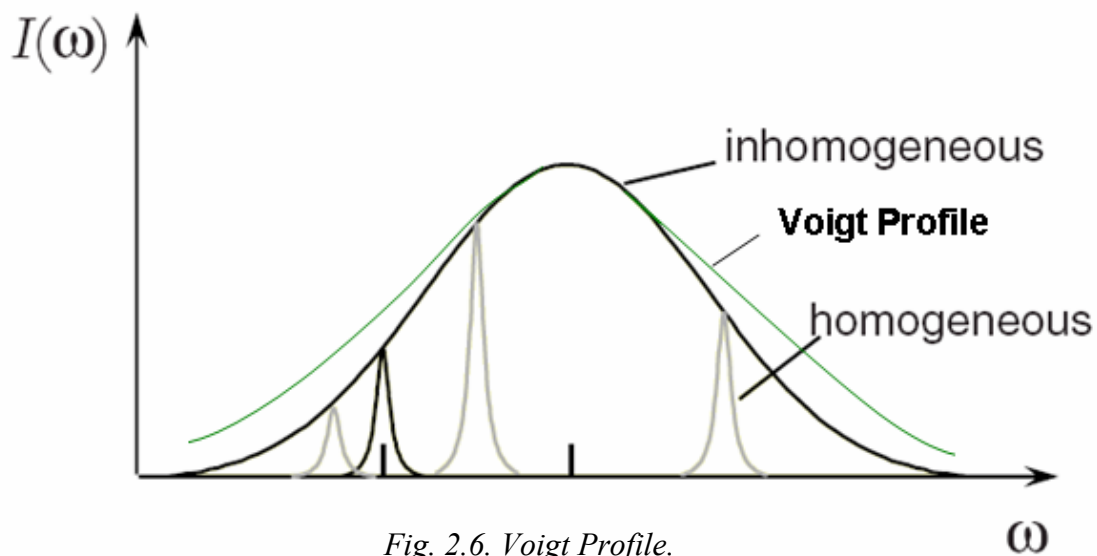
Fig. 2.6. Voigt Profile.

2.4. Doppler –free saturated Absorption spectroscopy.

The technique of Doppler-free saturated absorption spectroscopy was developed by the research group of Arthur L. Schawlow, who was one of the recipients of the 1981 Nobel Prize in physics for this work. Before the development of this technique, Doppler widths of about 500 MHz, caused by the random thermal motion of the atoms being studied, ultimately limited the resolution of optical spectroscopy. Doppler-free saturated absorption spectroscopy is insensitive to this effect. In this technique, there are two counter-propagating laser beams- a saturating beam and a probe beam. The saturating beam identifies a group of molecules in a narrow interval of axial velocities and pumps a sizable portion of the molecules from the lower level to upper one. It thereby creates hole in the velocity distribution of the lower level. A second laser beam, called a probe beam, is needed to probe this modified velocity distribution of molecules. When both saturating and probe beams are tuned to interact with the same group of molecules, the probe beam will experience a lower amount of absorption or a modified refractive index and therefore

a saturated absorption signal will emerge from the Doppler-broadened absorption background. The saturating field and probe beam generally influence each other but we have minimized that effect by working at lower probe power.

The effect of optical pumping on the saturation of population densities can be explained by simple two level systems in which the two levels are coupled to each other by absorption or emission and by relaxation processes as shown in Fig. 2.8. Such a two-level system is realized by many atomic resonance transitions without hyperfine structure.
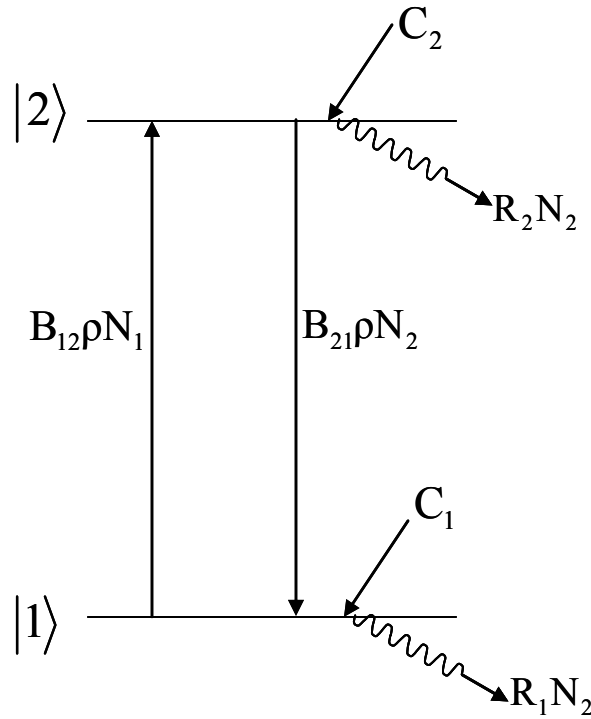
Fig. 2.7. Open two level system.

The absorption of the incident wave causes changes in the population of the levels involved in the absorbing transition. The rate equation for the population densities N_1 and N_2 of the non-degenerate levels $|1\rangle$ and $|2\rangle$ with statistical weight factors $g_1 = g_2 = 1$ can be written as,

$$\frac{dN_1}{dt} = B_{12}\rho_v (N_2 - N_1) - R_1 N_1 + C_1 \qquad [7a]$$

$$\frac{dN_2}{dt} = B_{12}\rho_v (N_1 - N_2) - R_2 N_2 + C_2 \qquad [7b]$$

where ρ_v is the spectral energy density of the radiation field, B_{12} and B_{21} are Einstein's coefficients, $R_1 N_1$ and $R_2 N_2$ are the total relaxation rate including spontaneous emission that depopulates the level $|1\rangle$ and $|2\rangle$, and C_1 and C_2 take care of all relaxation paths from other levels that contribute to the repopulation of both levels $|1\rangle$ and $|2\rangle$ as well as diffusion rate of molecules in both levels.

Generally, the quantities C_1 and C_2 are not noticeably changed by the radiation field. Under the stationary condition ($\frac{dN}{dt} = 0$), the unsaturated population difference for $\rho = 0$ can be written, using Eq.7, as

$$\Delta N^0 = \Delta N(\rho = 0) = N_2^0 - N_1^0 = \frac{C_2 R_1 - C_1 R_2}{R_1 R_2} \qquad [8]$$

And for the saturated population difference $(\rho \neq 0)$,

$$\Delta N = \frac{\Delta N^0}{1 + B_{12}\rho_v \left(1/R_1 + 1/R_2\right)} = \frac{\Delta N^0}{1 + S} \qquad [9]$$

where the saturation parameter

$$S = B_{12}\rho_v R^* = \frac{B_{12} I_v}{R^* . c}, \text{ with } R^* = \frac{R_1 R_2}{R_1 + R_2} \qquad [10]$$

gives the ratio of the induced transition probability $B_{12}\rho$ to the mean relaxation probability R^* and c is the velocity of light in medium.

The intensity $I=I_S$ at which the saturation parameter S becomes S=1 is called the saturation intensity. Using Eq. 10,

$$I_S = \frac{R*C}{B_{12}}$$ [11]

It is obvious from Eq. 9 that, for S=1, the population difference ΔN decreases to one half of its unsaturated value ΔN^0. Saturation also decreases the absorption coefficient $\alpha(\omega)$ by the factor (1+S) as shown in Fig. 2.9.

$$\alpha_s(\omega) = \frac{\alpha(\omega)}{1+S}$$
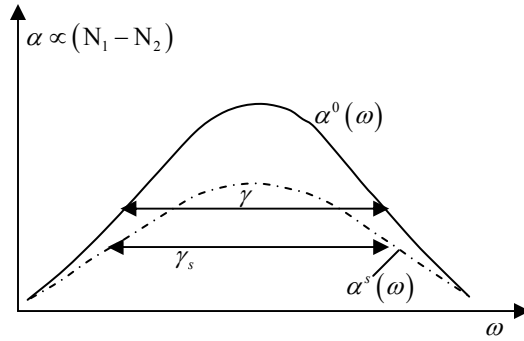
Fig. 2.8. Saturation absorption profile.

In two level system, the absorption cross-section of a molecule in level E_1 that moves with velocity v_z has a Lorentzian profile with natural line width γ given by,

$$\sigma_{12}(\omega, v_z) = \sigma_0 \frac{(\gamma/2)^2}{(\omega - \omega_0 - kv_z)^2 + (\gamma/2)^2}$$ [12]

where $\sigma_0 = \sigma(\omega = \omega_0 + kv_z)$ is the maximum absorption cross-section at the line center of the molecular transition.

Since the saturation parameter, $S(\omega, v_z)$ is proportional to absorption cross section, we can write,

14

$$S(\omega, v_z) = S_0 \frac{(\gamma/2)^2}{(\omega - \omega_0 - kv_z)^2 + (\gamma/2)^2} \qquad [13]$$

where $S_0 = S(\omega_0)$. The saturation parameter itself has a Lorentzian line profile and saturation is stronger at the line center than in the wings.

Due to the applied laser field, the population density, $N_1(v_z)dv_Z$ decreases in level $|1\rangle$ within the velocity interval $dv_Z = \gamma/k$ and the population density, $N_2(v_z)d_Z$ increases in level $|2\rangle$ correspondingly. From Eq. 9 and 13, we obtain,

$$N_2(\omega, v_z) = N_2^0 + \frac{\Delta N^0(v_z)}{\gamma_2^{\tau}} \left[\frac{S_0(\gamma/2)^2}{(\omega - \omega_0 - kv_z)^2 + (\gamma_s/2)^2} \right] \qquad [14]$$

$$N_1(\omega, v_z) = N_1^0 - \frac{\Delta N^0(v_z)}{\gamma_1^{\tau}} \left[\frac{S_0(\gamma/2)^2}{(\omega - \omega_0 - kv_z)^2 + (\gamma_s/2)^2} \right] \qquad [15]$$

where $\Delta N^0 = N_2^0 - N_1^0$ is the unsaturated population difference when the radiation field is zero. The homogeneous width of the transition is $\gamma = \gamma_1 + \gamma_2$. The longitudinal relaxation time, $\tau = \frac{1}{\gamma_1} + \frac{1}{\gamma_2}$ and the transverse relaxation time, $T = \frac{1}{\gamma_1 + \gamma_2} = \frac{1}{\gamma}$. For $\gamma_1 \neq \gamma_2$, the depth of the hole in $N_1(v_z)$ and height of the peak in $N_2(v_z)$ are different.

The saturated population difference, $\Delta N(v_z) = \frac{\Delta N^0(v_z)}{1 + S(\omega, v_z)}$

$$\Rightarrow \Delta N(v_z) = \Delta N^0(v_z) \left[1 - \frac{S_0(\gamma/2)^2}{(\omega - \omega_0 - kv_z)^2 + (\gamma_s/2)^2} \right] \qquad [16]$$

The velocity-selective minimum in the velocity distribution $\Delta N(\mathrm{v}_z)$ at $\mathrm{v}_z = (\omega - \omega_0)/k$ is often called the Bennet hole (Fig 2.10). It has a homogeneous width, $\gamma_S = \gamma\sqrt{1 + S_0}$ and a depth at the hole center at $\omega = \omega_0 + k\mathrm{v}_z$ of

$$\Delta N^0(\mathrm{v}_z) - \Delta N(\mathrm{v}_z) = \Delta N^0(\mathrm{v}_z)\frac{S_0}{1 + S_0} \qquad [17]$$
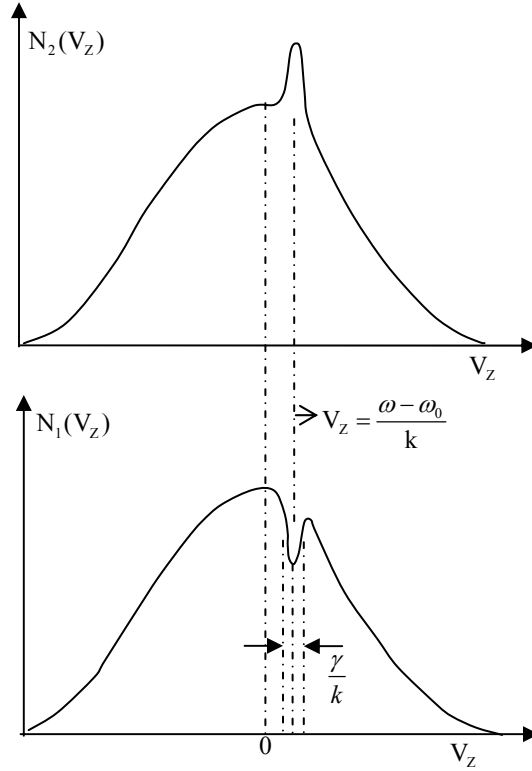
Fig. 2.9. Bennet hole in upper and lower state population distribution.

The total absorption coefficient caused by all molecules in the absorbing level is,

$$\alpha(\omega) = \int \Delta N(\mathrm{v}_z)\sigma_{12}(\omega, \mathrm{v}_z)d\mathrm{v}_z \qquad [18]$$

Here, despite the saturation, we again get the Voigt profile for $\alpha(\omega)$. For $S_0 < 1$, the Doppler width is generally large compared to the homogeneous width γ_S.

The saturated absorption coefficient can then be obtained by solving the above integral analytically with $v_z = (\omega - \omega_0)/k$, giving

$$\alpha_S(\omega) = \frac{\alpha^0(\omega_0)}{\sqrt{1+S_0}} \exp\left\{-\left[\frac{\omega - \omega_0}{0.6\delta\omega_D}\right]^2\right\} \qquad [19]$$

where the unsaturated absorption coefficient is given by $\alpha^0(\omega_0) = \Delta N^0 \dfrac{\sigma_0 \gamma c \sqrt{\pi}}{2v_P \omega_0}$

Equation 15 illustrates that: even though at each frequency ω the laser burns a Bennet hole into the velocity distribution N_1 (Vz), this hole cannot be detected just by tuning the laser through the absorption profile. The absorption coefficient,

$$\alpha_S(\omega) = \frac{\alpha^0(\omega)}{\sqrt{1+S_0}} \qquad [20]$$

of the inhomogeneous profile still shows a Voigt profile without any hole but is reduced by the constant factor $(1+S_0)^{-1/2}$, which is independent of ω.

The Bennet hole, however can be detected if two laser beams are used, the pump is fixed in frequency while the probe is scanned across the transition. This is also called a pump-probe saturated absorption scheme. In this scheme

1. The saturated pump laser with wave vector k_1 at the frequency ω_1 burns a hole into the velocity class $v_z \pm \Delta v_z / 2$ with $v_z = (\omega_0 - \omega_1)/k_1$ and $\Delta v_z = \gamma / k_1$.

2. A sufficiently weak probe laser with the wave vector k_2 at a frequency ω is tuned across the Voigt profile.

The integration of the absorption coefficient for the tunable probe laser over the velocity distribution gives

17

$$\alpha_S(\omega_1,\omega_2)=\alpha^0(\omega)\left[1-\frac{S_0}{\sqrt{1+S_0}}\frac{(\gamma/2)^2}{(\omega-\omega')^2+(\Gamma_s/2)^2}\right] \qquad [21]$$

where $\alpha^0(\omega)$ is the unsaturated Doppler profile with a saturation dip at the probe frequency, $\omega=\omega'=\omega_0\pm(\omega_1-\omega_0)k_1/k_2$. Sign $\pm$ holds for collinear and anticollinear propagation of the pump and probe waves. The FWHM $\Gamma_s=\gamma+\gamma_s=\gamma\left[1+(1+S_0)^{1/2}\right]$ of the absorption dip at $\omega=\omega'$ equals the sum of the width of the saturated dip due to strong pump beam and the unsaturated homogeneous absorption width γ of the weak probe beam. In general the linewidth of the molecular saturation is influenced by several broadening effects, such as transit time, pressure and power broadenings. We can express the overall linewidth as

$$\Gamma=(\Gamma_0+B_p.P)\sqrt{1+S} \qquad [22]$$

Where P is the gas pressure, B_p is the collision broadening coefficient, S is the saturation parameter, and Γ_0 is the remaining linewidth when both the gas pressure and optical power are sufficiently small. Γ_0 is basically transit time broadening.

When the pump and probe are simultaneously tuned, the detected dip is called a Lamb dip and is factor 2 narrower than in Eq 21. Therefore, we need to replace Γ_S with $\Gamma_S^*=\dfrac{\gamma+\gamma_S}{2}$ .i.e.

$$\Gamma_S^*=\frac{\gamma+\gamma_s}{2}=\frac{\gamma}{2}\left[1+(1+S_0)^{1/2}\right] \qquad [23]$$

The integration of the absorption coefficient in the case when both the pump and probe are simultaneously tuned over the velocity distribution gives,

$$\alpha_S(\omega) = \alpha^0(\omega_0) \exp\left\{-\left[\frac{\omega - \omega_0}{0.6\delta\omega_D}\right]^2\right\} \left[1 - \frac{S_0}{2(1+S_0)} \frac{(\gamma+\gamma_S)}{2\gamma_S} \frac{(\gamma_S/2)^2}{(\omega-\omega_0)^2 + (\Gamma_S^*/2)^2}\right]$$

If the intensity of the probe beam is very small as compared to the pump beam, we obtain formula similar to Eq. 21. For S<<1, $\gamma \approx \gamma_S$, we will get

$$\alpha_S(\omega) = \alpha^0(\omega)\left[1 - \frac{S_0}{2} \frac{(\gamma_S/2)^2}{(\omega-\omega_0)^2 + (\Gamma_S^*/2)^2}\right] \qquad [24]$$

This equation indicates that our experimental line profile with a narrow feature on top of a Doppler profile has the form of a Gaussian Profile times (1-Lorentzian Profile) as $\alpha^0(\omega)$ has Gaussian profile. If we subtract $\alpha^0(\omega)$ from $\alpha_S(\omega)$, we will get line shape for narrow feature which would be a narrow Lorentzian times a broad Gaussian.

Considering the form of the equation above, we have fitted our line shape with the similar kind of function in Origin software. Our exact fitting expression in the Origin software is,

$$Y = Y_0 + A_g \exp\left[\frac{-2(X - X_{cg})}{\omega_g}\right]^2 \left[1 - A_l \frac{\omega_l^2}{4(X - X_{cl})^2 + \omega_l^2}\right] \qquad [25]$$

where A_g is the amplitude of the Gaussian Profile, Ag times Al gives the amplitude of the narrow feature on top of Gaussian profile, X_{cg} and X_{cl} are the peak values of the two peaks, ω_g and ω_l are the width of the profiles.

CHAPTER 3

Molecular spectroscopy of acetylene

The infrared range of the spectrum covers wavelengths $\lambda = 1\text{–}25\ \mu m$, or energies per photon $E = hc/\lambda$, expressed in "wave number" (cm^{-1}) units as $E/hc = 1/\lambda = 400\text{–}5000\ cm^{-1}$, where h is Planck's constant and c is the speed of light. Infrared spectroscopy probes the vibrational and rotational energy levels of molecules. Acetylene $^{12}C_2H_2$ has large number of rotational and vibrational transitions between 1510 nm and 1540 nm and has importance through the provision of a number of standards covering the telecommunications window near $1.5\ \mu m$.

Classically, molecules absorb infrared light because the oscillating electric field of the light drives polar vibrational modes. Power from the oscillating electric field is absorbed by the vibrations most efficiently when the light frequency matches the resonant vibrational frequency. Thus the absorption spectrum has peaks which match the molecular-vibrational frequencies. Quantum mechanically, light absorption leads to transitions between different vibrational energy levels. However, not all transitions between vibrational levels are "allowed." Each allowed transition results in an absorption line in the IR spectrum. The $\Delta J = -1$ and $\Delta J = +1$ transitions are referred to as P- and R-branch lines respectively and are shown in Fig. 3.1. Rotational and vibrational motions are coupled because vibrations change the moment of inertia of the molecule and hence affect the rotations.

Transitions from the ground state to the first excited state of a normal mode lead to fundamental bands in a spectrum. Transitions from a ground state to the second excited

state (or higher) lead to "overtone" bands. In polyatomic molecules, one photon may also excite more than one vibrational mode simultaneously. Bands arising from these transitions are called "combination" bands. Finally, often not all molecules at room temperature are in the ground vibrational state, and vibrational bands called "hot bands" may arise from a transition from one excited vibrational state to another.
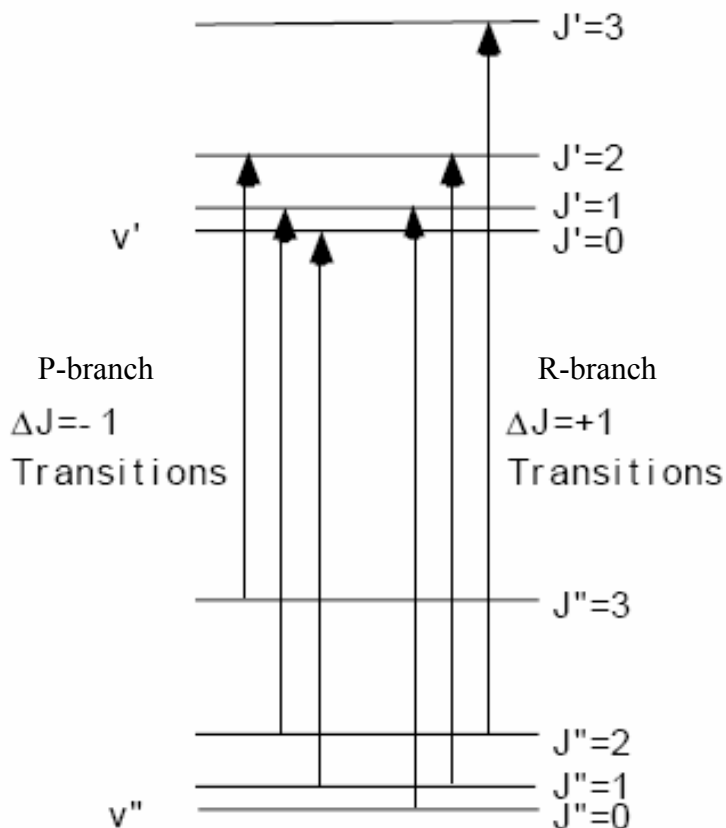

Fig. 3.1. P- and R- branches in transition lines of acetylene. Figure taken from Ref[16]

A molecule composed of N-atoms has 3N degrees of freedom, six of which are translations and rotations of the molecule itself. This leaves 3N-6 degrees of vibrational

freedom (3N-5 if the molecule is linear). Acetylene has $3N - 5 = (3)(4) - 5 = 7$ normal modes of vibration, only five of which have independent frequencies (Fig 3.2).
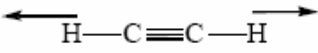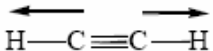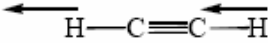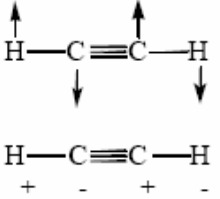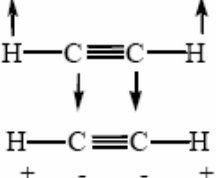
Mode	Description	Normal Mode
ν_1	Symmetric C-H stretch	H—C≡C—H
ν_2	Symmetric CC stretch	H—C≡C—H
ν_3	Asymmetric C-H stretch	H—C≡C—H
ν_4	Symmetric bend	H—C≡C—H H—C≡C—H + - + -
ν_5	Asymmetric bend	H—C≡C—H H—C≡C—H + - - +

Fig. 3.2. Fundamental vibrational mode of acetylene. Figure taken from Ref[16]

There are two doubly degenerate (equal-energy) bending vibrations. Among these five frequencies, there are two labeled ν_1 and ν_3 that arise from primarily CH stretching motions. We are examining the combination band, $\nu_1 + \nu_3$ which arises from simultaneous (by a single quantum) excitation of the ν_1 and the ν_3 modes plus allowed rotational energy changes ($\Delta J = \pm 1$). The $\nu_1 + \nu_3$ combination band results in a parallel dipole moment

oscillation and hence gives rise to a parallel band which one may easily assign and analyze. Note the interesting point that while excitation of the υ_1 mode alone is dipole-forbidden, it can be excited in combination with the dipole-allowed υ_3 mode excitation.

In acetylene, there is no hyperfine structure and so we only observe one peak within each Doppler-broadened transition. The $v_1 + v_3$ combination band of $^{12}C_2H_2$ has more than 50 strong absorption lines in the 1520-1550 nm regions.

$v_1(cm^{-1})$	$v_3\,(cm^{-1})$
3373.7	3278

Table 1. Pure Vibrational Energies of $^{12}C_2H_2$.

The natural line width of a molecular transition between two vibrational levels of the electronic ground state with a wavelength in the infrared region is very small because of the long spontaneous lifetime of vibrational levels. For a typical lifetime of 10^{-3}s the natural linewidth is 160 Hz.

3.1. Calculation of different types of line shape broadening in acetylene.

A spectral line always has an inherent width produced by uncertainty in atomic energy levels which arises from the finite length of time involved in the radiation process, through the Heisenberg uncertainty principle. However, the intrinsic linewidth predicted by the Heisenberg uncertainty principle is rarely observed because of several other broadening mechanisms. The broadening effect increases the width of the spectral lines. The most important of these broadening effects are shown below.

3.2. Transit-time broadening with a Gaussian beam.

The interaction time of the molecule with the radiation field contributes to the broadening of the spectral line, through a mechanism called transit time broadening. In

smaller core fiber, the interaction time is very small as compared to the spontaneous lifetime of the ro-vibrational states. Therefore, the broadening due to transit time completely dominates the life time broadening. In our experiment, transit time broadening could be the major source of broadening of the sub Doppler profile.

Consider a Gaussian laser beam which is propagating along the z-direction. The wave surface is planar at its beam waist. The field distribution there is written as,

$$E(x, y, t) = E_0 \exp(-r^2 / w^2) \cos \omega t \qquad [25]$$

Where, $r^2 = x^2 + y^2$ and w is the beam width.

Then the autocorrelation function of the field as seen by the atom traversing the beam with the velocity v is calculated by using $r^2 = v^2 t^2 + a^2$ to be proportional to $\exp\left[-(\omega - \omega_0)^2 \dfrac{w^2}{2v^2}\right] \cos \omega t$, where 'a' is the minimum distance of the atom from the beam axis. The frequencies observed by the molecule are obtained by taking a Fourier transform of the autocorrelation function. The Fourier transform gives a Gaussian line shape with intensity profile,

$$I = I_0 \exp\left[-(\omega - \omega_0)^2 \frac{w^2}{2v^2}\right] \qquad [26]$$

which immediately gives transit time linewidth(FWHM)

$$\Delta \omega = 2\sqrt{2 \ln 2}\,(v / w) \qquad [27]$$

In terms of the beam diameter, D=2w,

$$\Delta \omega = 2\sqrt{2 \ln 2}\,(2v / D) = 4.71v/D$$

In terms of frequency,

$$\Delta v = 0.75v / D \qquad [28]$$

But the most probable velocity of molecules in a Maxwell-Boltzmann velocity distribution is given by

$$v_p = \sqrt{\frac{2RT}{M}} \qquad\qquad [29]$$

where M is the molar mass.

For $^{12}C_2H_2$, M=26.016 g/mole; Room Temp, T=295^{0}K

$$V_p \approx 434 m/s$$

$\Rightarrow \Delta v \cong 25\text{MHz}$ for 13x10^{-6}m laser beam mode field diameter which is the case for the 20 μm diameter hollow core PBG fiber.

3.3. Collision Broadening.

The collision of molecules causes molecules in the excited state to revert to the ground state. Collisions thus shorten the lifetimes of excited states and lead to the broadening of the associated spectral lines. As the gas pressure is increased from some arbitrarily small value, the shape and width of a spectral line is affected by intermolecular collisions. Generally, the linewidth increases due to collisions between molecules. When the pressure is very high the collisional broadening becomes dominant over Doppler broadening, and then the line shape becomes Lorentzian. The collisional broadening is often called pressure broadening. We have experimentally measured the pressure broadening for the different lines under different physical conditions. The pressure broadening is almost the same for the different lines and found to be approximately equal to 11 MHz/Torr.

3.4. Saturation and power broadening.

In saturation spectroscopy, the signal comes from the molecules that have experienced a certain degree of saturation from the laser field, usually characterized by the saturation parameter S. If the pump beam intensity is high enough, the ground state is significantly depleted and therefore absorption of the probe beam is reduced compared to the case without the pump beam. For the intensity equal to or more than saturation intensity, half of the molecules, on average, are in the excited states. This is called the saturation of the molecular transition. This results in a noticeable decrease of the population in the absorbing levels. This saturation of the population densities also causes additional line broadening called saturation broadening.

The saturation parameter S can be written as $S = \dfrac{I}{I_s}$, where I_s is the saturation intensity. The width of the saturation-broadened line, γ_s increases with the saturation parameter, S at the line center as,

$$\gamma_s = \gamma\sqrt{1+S} \qquad\qquad [30]$$

When pressure is very low (<50 mT), the width of the saturation signal is dominated by the transit time broadening which is ultimately governed by the diameter of the laser beam and therefore depends upon the diameter of the hollow core of the fiber. In this case, we can express saturation intensity in terms of transit time width, Γ_t

$$I_s = \frac{\varepsilon_0 c\hbar^2}{2\mu^2}\Gamma_t^{\,2} \qquad\qquad [31]$$

where μ is the transition dipole moment.

Equation 31 shows the dependence of the saturation intensity on transit-time broadening and therefore upon the square of the diameter of the core of the fiber.

$$\text{i.e. } I_s \propto \Gamma_t^{\ 2} \propto \frac{1}{d^2}$$

but the intensity inside the fiber can be written as, $I = \dfrac{\text{Power}(P)}{\pi d^2 / 4}$

This implies that saturation parameter, $S = \dfrac{I}{I_s}$ is independent of the size of the fiber.

Therefore saturation spectroscopy in the transit-time limited region is characterized by saturation power rather than saturation intensity I_s.

When pressure broadening, Γ_p exceeds the transit time broadening, Γ_t then we can write saturation intensity as

$$I_s = \frac{\varepsilon_0 c \hbar^2}{2\mu^2} \Gamma_p^{\ 2} \tag{32}$$

In this case, the saturation parameter, S does depend upon the diameter of the fiber,

$$\text{i.e. } S = \frac{I}{I_s} \propto \frac{1}{d^2}$$

Saturation power of 330mW is required to saturate the molecule at the pressure of 50 mT inside a fiber with beam size of 440 μm diameter [2]. If we have 30 mW of power output from the fiber then saturation parameter, S is given by,

$$S = \frac{I}{I_s} = \frac{P}{P_S} = \frac{30mW}{330mW} \approx 0.1 \text{ (low)}$$

It clearly indicates that we need to have either very high power to saturate or we need very long fiber filled with very small pressure to see the same signal. But ordinary hollow

fibers are inherently leaky, and one cannot get more than 40% output in 1 m length, and losses are very large. Therefore it is very difficult to see the saturation signal.

CHAPTER 4

Photonic band gap fiber

For the first time back in 1996, J.C. Knight et al. reported the fabrication of a new type of optical waveguide with cladding where air holes were arranged in a two dimensional periodic structure in glass: the photonic crystal fiber [11]. Guiding of light through these fibers is not due to total internal reflection of light as in conventional fiber but due to existence of the photonic band gap (PBG) in the transmission spectrum of the fiber. Hollow fibers that lack the PBG, such as hollow capillary tubes, use external reflection and are thus inherently leaky. They have additional losses on bending. Furthermore, they invariably support many different transverse modes; that is, they are highly multimode.
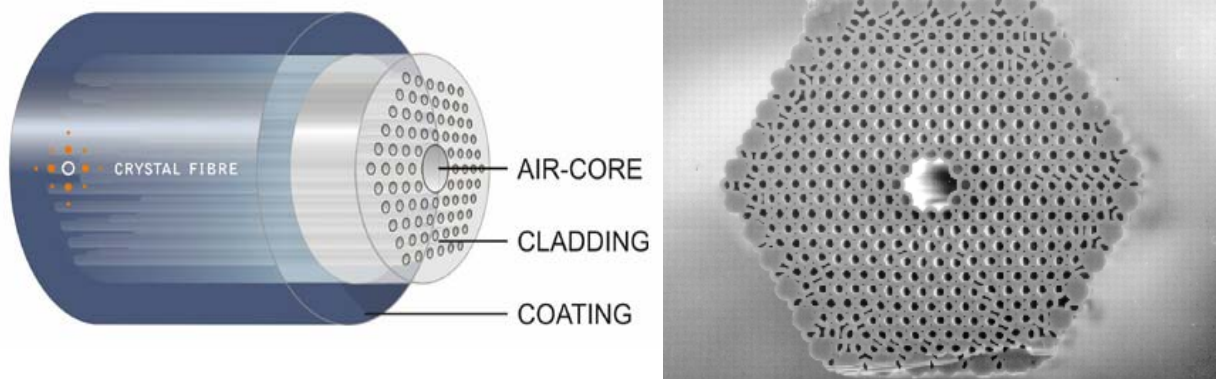
Blaze Photonics
(www.blazephotonics.com)   J. C. Knight et al., Science, 282, 1476, 1998

Fig.4.1. photonic band gap fiber.

But a PBG fiber allows the spectral region of single mode wave guiding to be considerably expanded. In fact, the cladding of a holey fiber thus produced by periodic arrangement of air holes in glass displays a photonic band gap for a certain wave vector. Within the corresponding frequency ranges, radiation cannot penetrate into the fiber cladding. The fiber core can be considered as a lattice defect in an otherwise perfect two dimensional photonic crystal. Ideally a photonic band gap fiber can be single mode for all wavelengths [17]. For more detail review see 'Holey fibers' by A M Zheltikov[18].

CHAPTER 5

Experimental Set-Up

There are various ways to perform saturation spectroscopy. It can be done in a vapor cell but it requires high intensities over long lengths. Therefore power build-up cavities are frequently employed. To the best of my knowledge, people are also doing saturation spectroscopy in capillary tubes [19]. These tubes support many different transverse modes, and are highly multimode. Since capillary tubes are also inherently leaky and suffer lots of bending loss, extremely large lengths (~km's) of capillary tubing filled with very low pressure filled inside would be required to saturate the molecules. We are doing saturation spectroscopy in photonic band gap fiber which has very low loss (~3%) in near infrared region. They are also fairly insensible to bending loss, and they also allow the spectral region of single mode wave guiding to be considerably expanded. These PBG fibers have already been used as a fiber gas cell [20], but never before in a counter-propagating geometry. Here we use a high-power pump beam and a low-power probe beam, so the effect of the probe can be assumed to interrogate the sample in a linear fashion; the probe beam does not influence the saturating field.

The experiment setup is shown in Fig. 5.1. In this experiment we have used a commercially tunable diode laser from SANTEC Company. The grating inside the laser is mounted on a piezo which can be controlled by applying a voltage ramp. The frequency of the laser is not fixed; rather it is being swept by the triangle waveform applied to the piezo of the tunable diode laser. We have used a signal generator (not shown in Fig. 5.1) to control the voltage ramp. We can control the overall frequency offset and the amplitude of the sweep with the help of the signal generator.
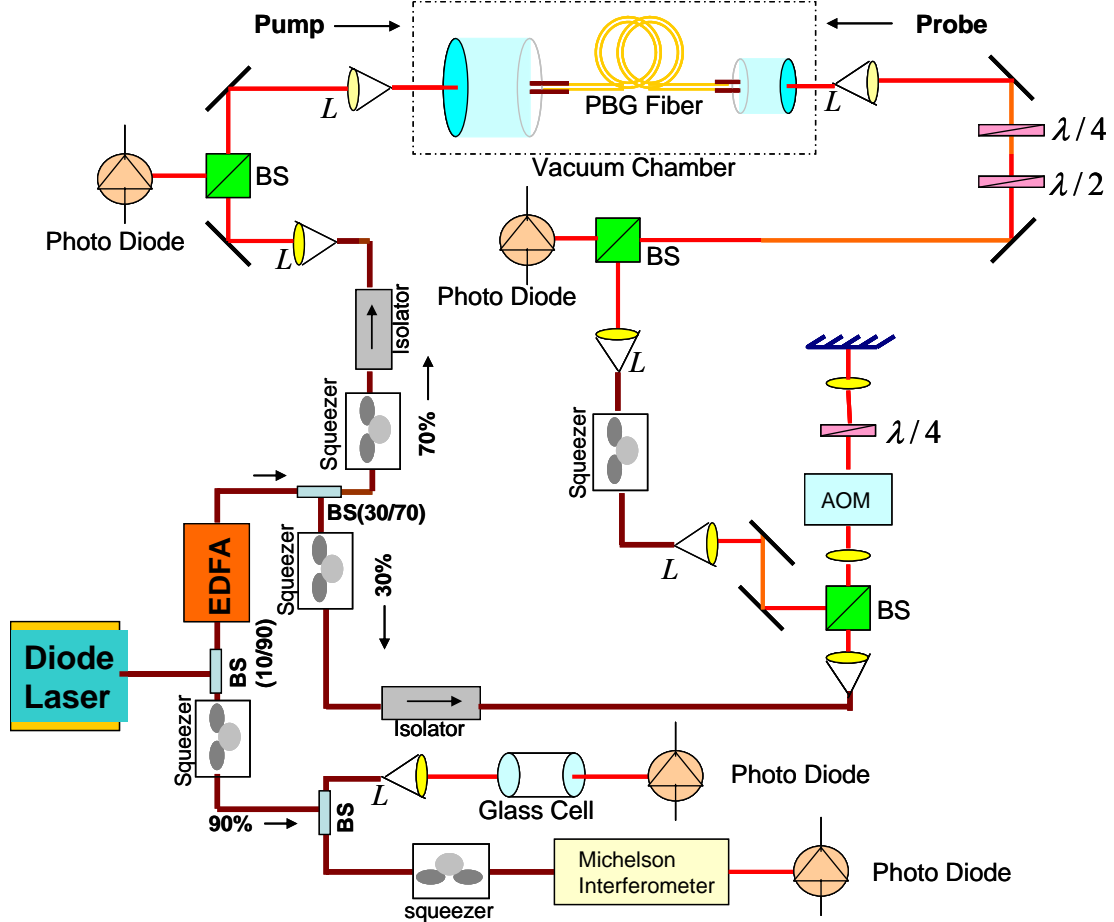
Fig.5.1. Apparatus for Doppler-free saturated absorption spectroscopy of acetylene.

The output power of around 5 mW from the tunable diode laser is split into two beams in a ratio of 10:90 using a beam-splitter. The less intense beam enters an EDFA and gets amplified up to 450 mW. The more intense beam is divided between a Michelson interferometer and an acetylene-filled glass cell. The combination of the squeezer and the beam splitter divides the intensity between the Michelson interferometer and the glass cell in a controllable ratio.

The glass cell of about 5 cm length is filled with acetylene at a pressure of about 50 Torr. The glass cell mimics a NIST cell[6]. The beam through the glass cell is detected

by a photodiode. The signal from the glass cell is a linear absorption signal, and the spectral lines are Doppler-broadened and pressure broadened.

A Michelson interferometer is used to calibrate the horizontal axis of the oscilloscope in optical frequency units. The laser beam is divided by a beam splitter and two beams are recombined at the beam splitter and detected by a photodetector after the beams have traveled distances of $2L_1$ and $2L_2$ (as shown in Fig 5.2). After returning to the beam splitter, the two beams will have a phase difference due to their path differences. As the laser frequency is scanned, this phase difference will change, causing a series of maxima and minima.

The frequency spacing of the resolution maxima is given by,

$$\Delta \upsilon = \frac{c}{2(L_1 - L_2)}$$

This expression clearly shows that the resolution of the interferometer is governed by the difference in the arm length.
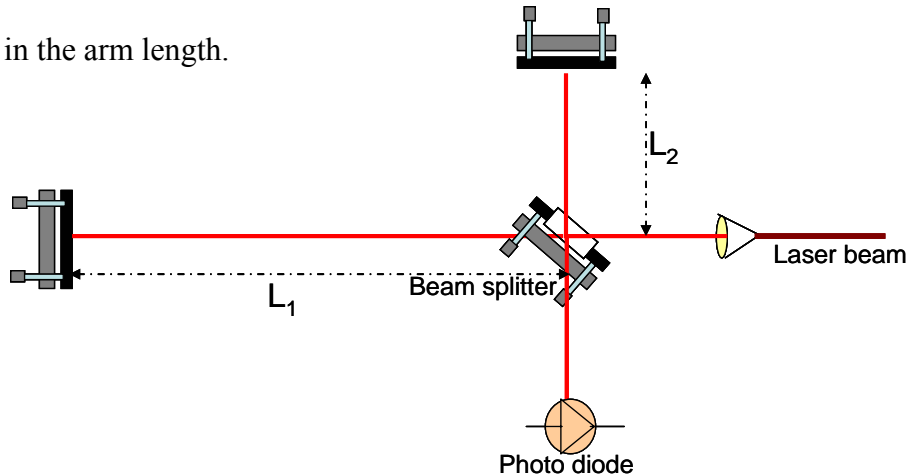

Fig.5.2. Michelson Interferometer.

The output beam from the EDFA is split into a low intensity probe beam and a high intensity pump beam by using a 30/70 beam splitter. The low intensity beam further undergoes double-passing through an acousto-optic modulator (AOM) and is used as the probe beam. The un-shifted beam is blocked on each pass using an opaque metallic

block. The presence of an AOM, in fact, minimizes interference between the probe beam and scattered pump beam light that reflects off the end of the fiber and then strikes the photodetector. The frequency of the probe beam is shifted by 43.2 MHz on each pass. So there is a total of 86.4 MHz of shift in the frequency as compared to the pump beam. This is in fact one of the techniques to create an offset between the pump and probe beams in saturation spectroscopy. The quarter wave plate and the half wave plate correct for the polarization rotation that occurs inside the fiber so that the pump and probe beam can be perfectly separated.

Now, we focus the pump and probe beams into the photonic band gap fiber placed inside the vacuum chamber. The vacuum chamber consists of two separate parts, connected to each other only through the photonic band gap hollow core fiber (PBG Fiber). A long PBG fiber is kept inside two hollow metal tubes. Two extreme ends of the stripped and nicely cleaved small portion of fiber are just outside the metal tube as shown in Fig. 5.3.
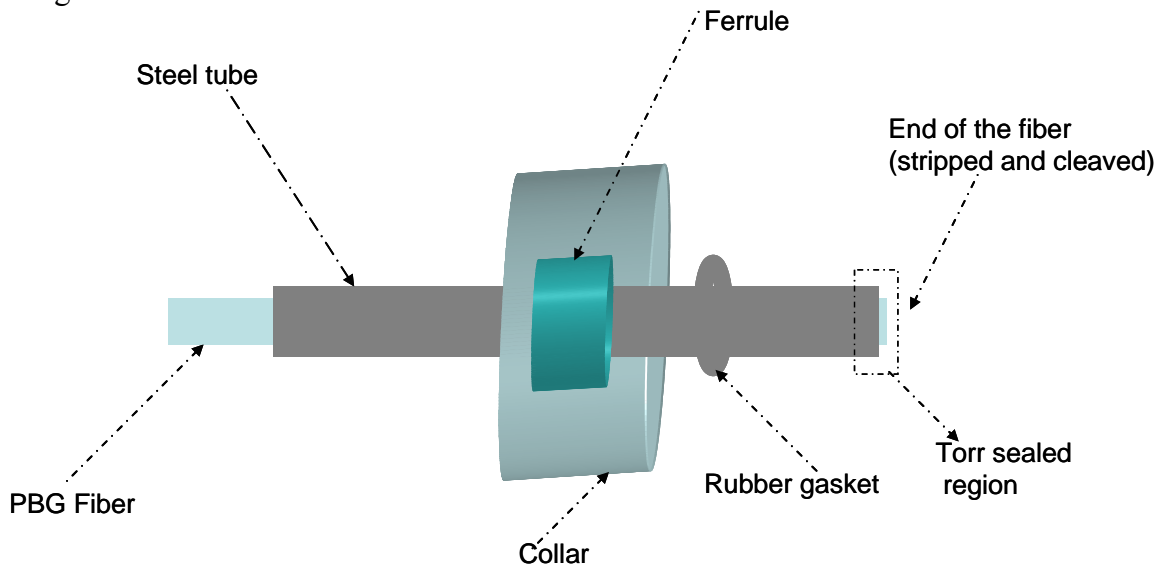

Fig. 5.3. Compression Fitting.

An epoxy such as 'Torr Seal' is used to create a vacuum seal between the fiber and the hollow metal tube. The metal tube is in turn sealed to two separated vacuum chambers by compression fittings. Gas is then introduced into both sides of the already evacuated chambers so that an equilibrium state of pressure inside the fiber is reached quickly.

CHAPTER 6

Data Analysis

This chapter presents the direct experimental results showing various line shapes in different pressure and power regions. Three molecular overtone bands, P (11), P (13) and P (16) have been analyzed. The observed resonance linewidth is analyzed and attributed to various broadening mechanisms in the experiment. A simplified diagram of non-linear spectroscopy is shown in Fig. 6.1 below.
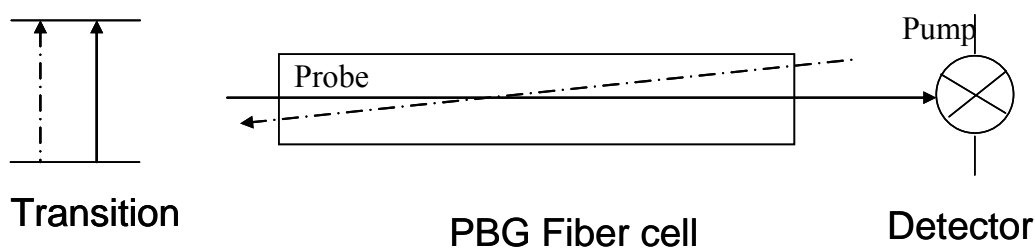

Fig. 6.1. The radiation reaching the detector is dependent on both beams.

The two counter-propagating waves interact with the same atoms. The beam propagating to the right causes the transitions indicated with a dashed line in the energy level diagram, and the beam propagating to the left, the 'probe beam', causes the transition indicated with a solid line. In this case, the field reaching the probe is a function of both fields. The pump beam changes the population of the atomic states and the probe detects these changes.

By tuning the diode laser to different wavelengths, we have probed different ro-vibrational lines in the $^{12}C_2H_2$ overtone band. We can gain important information from the relative intensities of the transition. The intensity of an absorption line is proportional to both the number of molecules in the particular initial state and the strength or transition moment of the particular transition. The transition moment can be thought of as the

probability that a molecule interacting with light of the appropriate frequency will actually absorb a photon and undergo a transition. We have digitally recorded the molecular resonance lineshape with an oscilloscope as shown in Fig. 6.2 below.
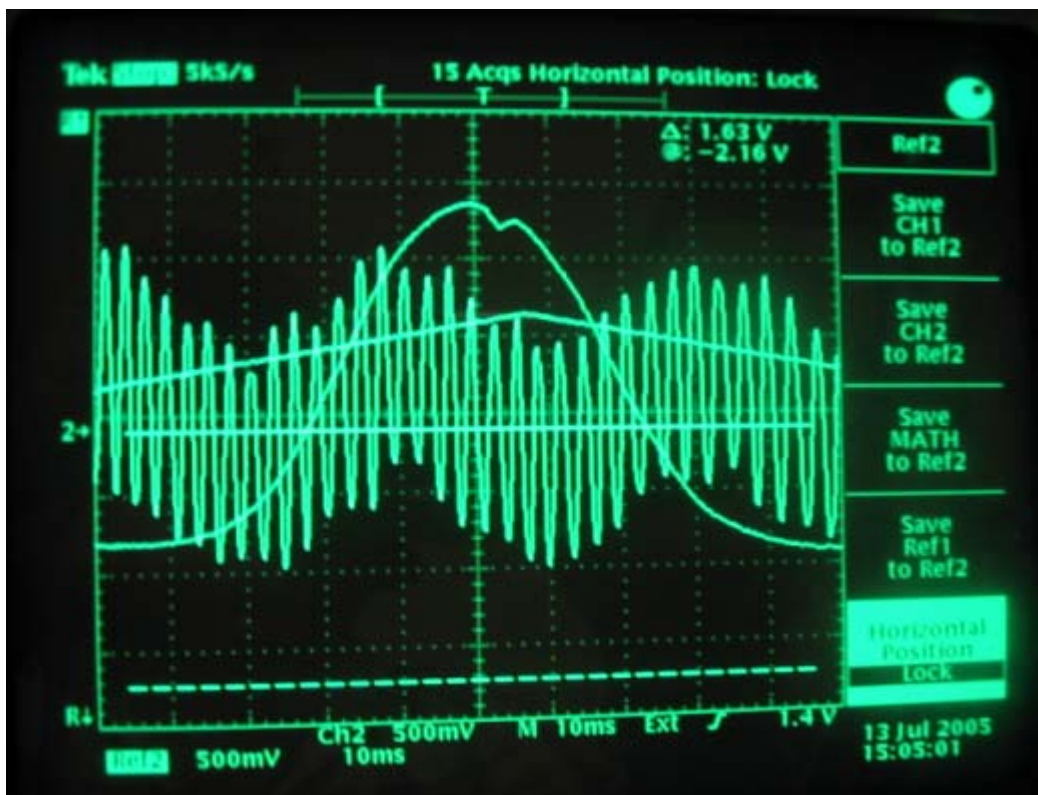

Fig. 6.2. Actual picture of the saturation spectrum of the P (11) feature at pressure of ~1 Torr and the Michelson fringes to linearize the sweep. The triangular ramp function was taken at a later time.

The observed lineshape is analyzed with the help of the advanced fitting techniques in Microcal Origin software. We have carried out a series of experiments studying the line shape. In particular, the P (11) line has been extensively used for the lineshape and linewidth studies. The different absorption curves taken are averaged together and fitted with Eq. 24. The error estimates are the error returned by the χ^2

fitting routine in Origin. The horizontal time axis of the lineshape has been calibrated using the fringes of a Michelson interferometer.

The experimentally measured absorption spectra are shown in Fig. 6.3a. The curve is normalized to unit intensity at resonance. The probe beam was frequency- shifted by more than 40 MHz by using an acousto-optic modulator to avoid possible interference
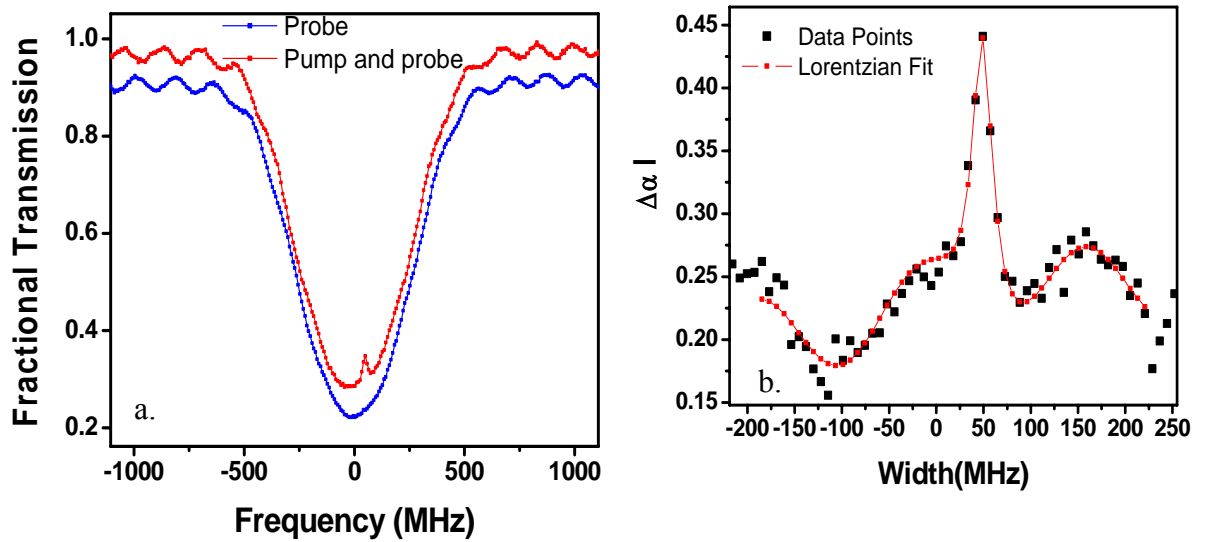

Fig. 6.3. (a). Saturation absorption spectrum of the P(11) with the narrow feature. Pump laser power of 33 mW was coupled into 35 cm long fiber with a core size 20 μm, containing acetylene gas at 800 mT of pressure. The large background noise has periodic behavior, indicating an etalon effect or interference. (b). Lorentzian fit of the absorption coefficient with a FWHM of 27 MHz

between the pump and probe beam. This is why the narrow feature shown on top of the Doppler background is shifted from the center of the Doppler peak. The line shape in Fig. 6.3a has a lot of observable background noise. We have figured out that a certain portion of the pump beam gets reflected back and interferes with the probe beam and

38

produces noise. To avoid that, we have placed a quarter-wave plate and a half-wave plate between the two mirrors in the probe side. The quarter-wave plate converts the circular polarization to linear polarization while the half-wave plate rotates the linear polarization of the laser beam so that the polarization of the pump and probe are always perpendicular to each other, and the unwanted reflected pump beam is prevented from striking the photo detector of interest. It is essential to control the polarization of both the pump and probe beams to get high Signal-to-noise ratio (SNR).

Figure 6.4 below shows the same P (11) line which has been taken three month after we took spectra shown in Fig. 6.3 in similar physical conditions. By suitable control of polarization and careful alignment of the optical path, we are able to reduce the background noise significantly.
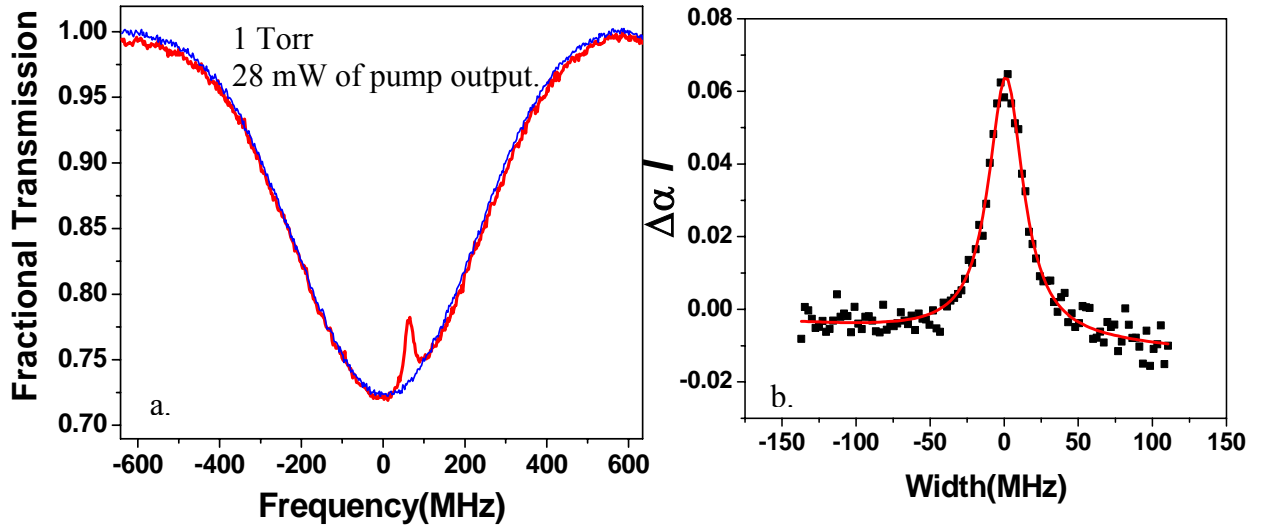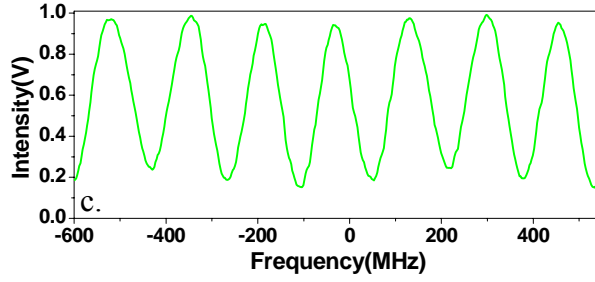

Fig. 6.4. (a) Saturation absorption spectrum of P (11). (b) Lorentzian fit of Doppler free saturated spectral line.

(c) Michelson interferometer fringes to calibrate the horizontal axis of the oscilloscope in frequency units.

In the beginning, we treated the narrow feature on top of the Gaussian profile as a pure Lorentzian. To get the narrow feature, we simply subtracted the probe signal from the "pump and probe" signal and fitted $\alpha(\omega)$, in $I(\omega) = I_0 \exp[-\alpha(\omega)L]$, with a Lorentzian as shown in Eq. 8 above. In the absence of the pump beam, $\alpha = \alpha_D$ is a Doppler-broadened signal. With the pump, $\alpha = \alpha_s$ is a sub-Doppler profile, and the difference $\Delta\alpha(\omega) = (\alpha_s - \alpha_D)$ gives the signal of interest.

More detailed study showed that the narrow feature cannot be strictly Lorentzian as we have treated it above. Instead, it should be a product of Lorentzian and a Gaussian. So, rather than subtracting the "probe" signals from the "pump and probe", we have fitted the whole saturation profile with the theoretical model as given in Eq. 25 above.

Figure 6.5 below shows the saturation spectrum of the P (11) feature as a function of pressure. Each signal represents the average of 8 sweeps across the transition. It can be clearly seen that the SNR is very large.
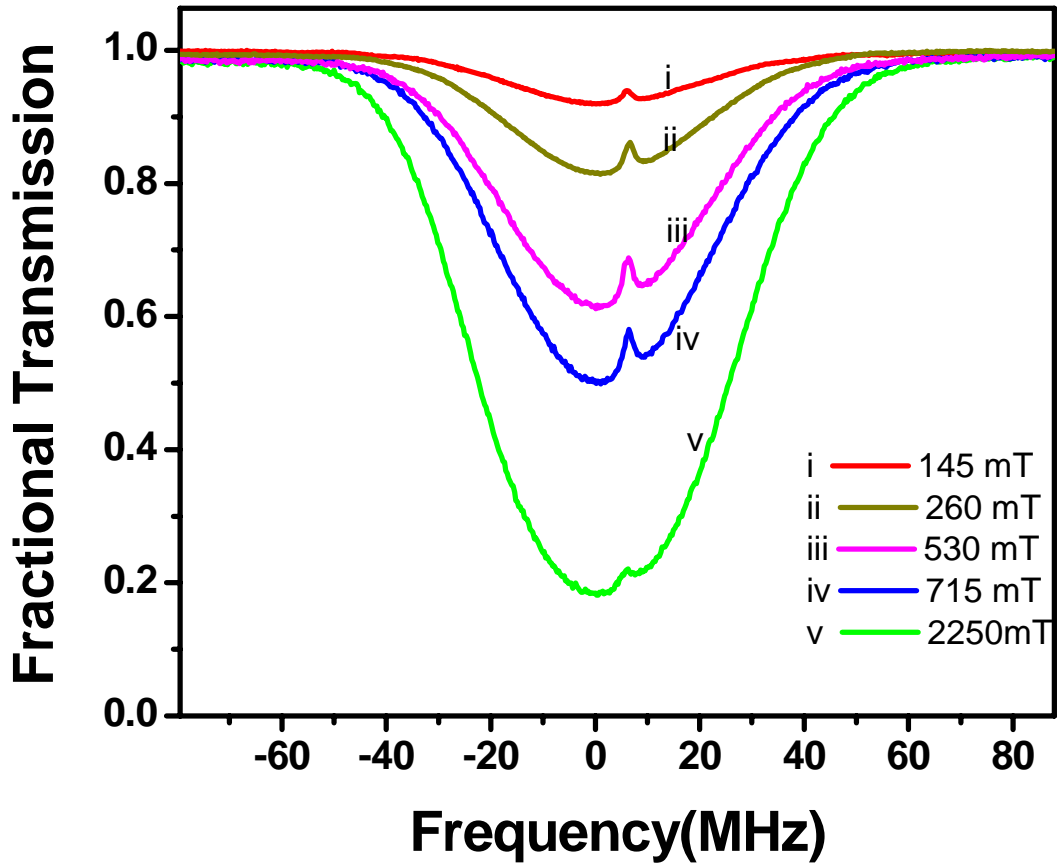

Fig. 6.5. Saturated absorption spectra of P (11) feature as a function of 5 different pressures. Each curve is normalized to unit intensity at resonance. The zero point in the frequency scale is adjusted so that the origin of the frequency is at the line of symmetry of the Doppler-broadened curve.

Figure 6.6 below shows the theoretical best fit for the absorption profile as shown in Fig. 6.5. The dots in different color represent the experimental absorption spectrum and the solid curve is a best theoretical fit. The theoretical fit curves fit well to the experimental curves.
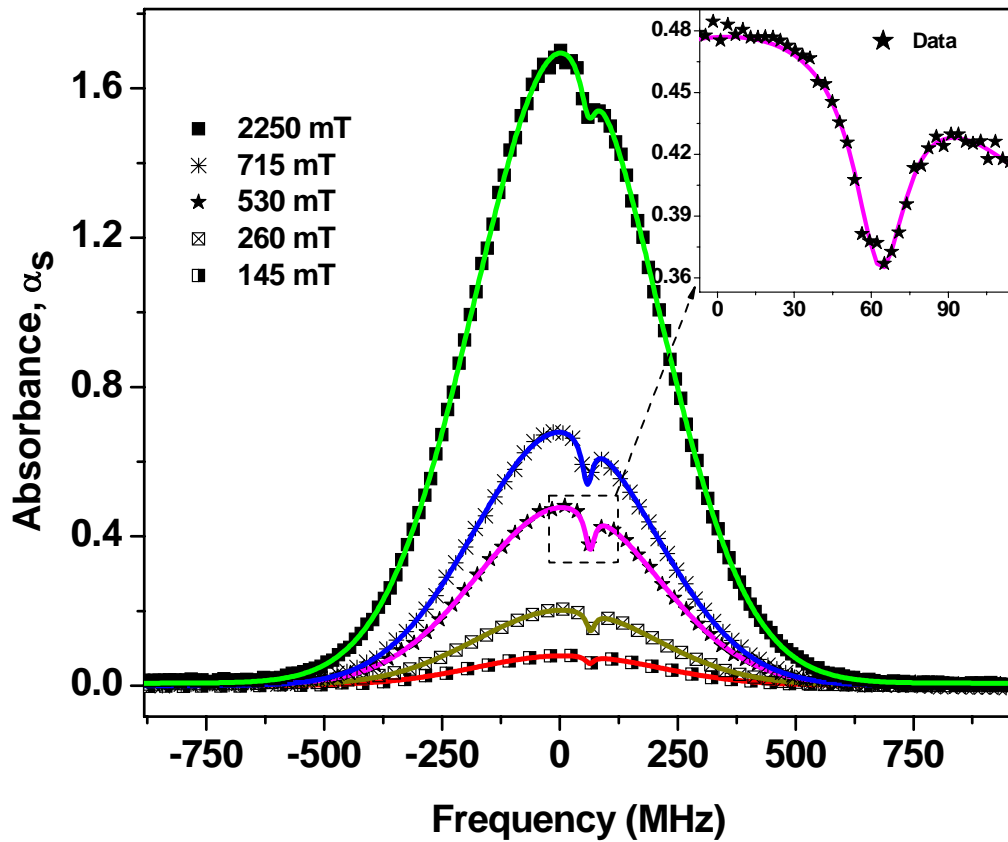
Fig. 6.6. Frequency scan of the $\alpha_S(v)$, calculated from measurements shown in Fig. 6.5, of P (11) transition line shape and overlaid theoretical fit based on the broadening formalism explained in Eq 24. The fit result also produces information such as the amplitude of the Gaussian profile, amplitude of the small peak on top of the Gaussian, and width of both.

To establish a stable and reproducible frequency standard, we need to understand all of its operating parameters. For a molecular reference operating at a certain pressure, it is important to study the pressure- and power- dependent linewidth broadening.

The pressure broadening of $^{12}C_2H_2$, P (11) and P (13) transitions is carried out in a ~80 cm long PBG-fiber. The gas pressure is limited in the range of 150 mT to 2250 mT. The output power from the fiber was kept at 29 mW with a coupling efficiency of ~70%

for P(11) whereas the output power for P(13) was 14 mW with ~65% coupling efficiency. As we change the gas pressure inside the fiber, we witness linewidth broadening for different peaks.
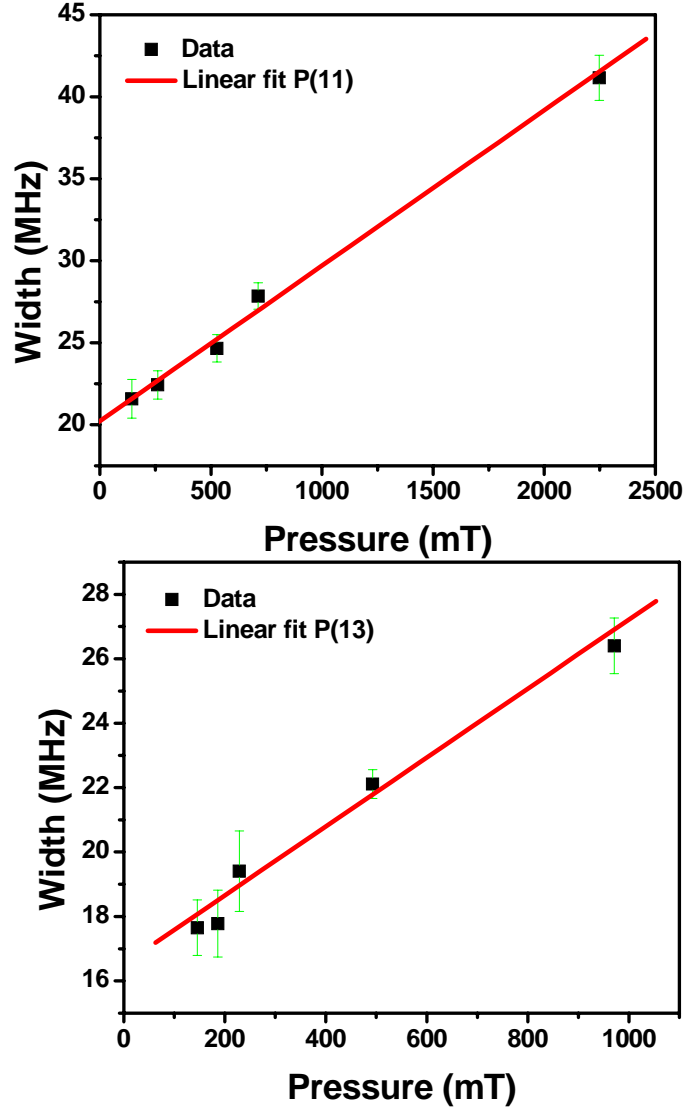

Fig. 6.7. Pressure-Broadening measurement of the P (11) line at 29 mW and P (13) at line 14 mW.

Extrapolated to zero pressure, we calculated the transit time broadening of both the P(11) and P(13) lines at pump powers of 29 and 14 mW. The zero-pressure linewidth of the P(11) and P(13) line is 17 MHz and 21 MHz respectively (Fig 6.7).

Fig. 6.8 below shows the effect of power on the experimentally observed saturation line shape for the P (11) line at a constant pressure of 1 Torr. We can see that
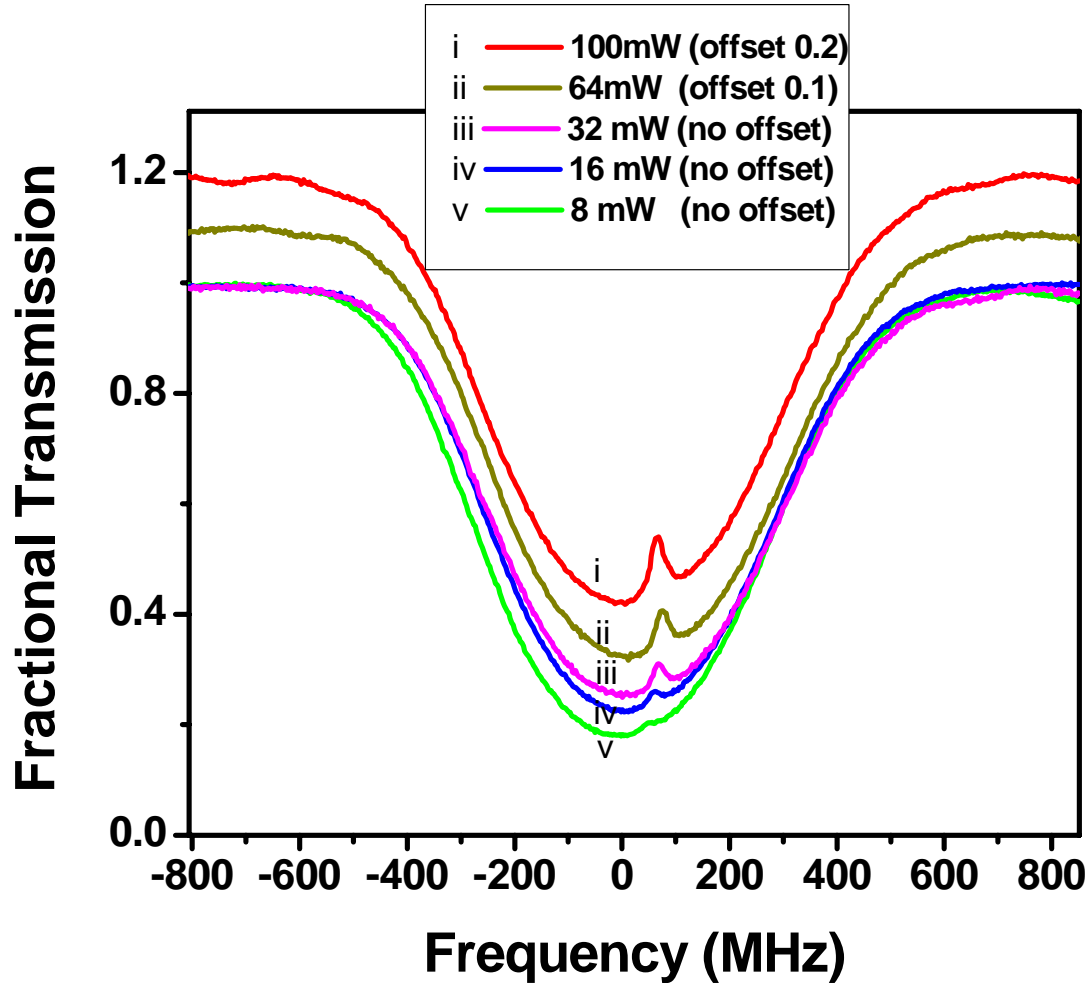
Fig. 6.8. Power broadening effect on the lineshape for P (11) lines at the constant pressure of 1 Torr. Each curve is normalized to unit intensity at resonance.

as the power is reduced to smaller values, there is significant decrease in the amplitude of the narrow feature on top of the Doppler profile.

Figure 6.9 below shows the power broadening effect on the width of the sub-Doppler profile. It seems that there is not much effect due to the pump power on the width of the narrow feature. Saturation power at the pressure of 1 Torr inside the 20

micron PBG fiber is found to be 44 mW, which is more than 6 times smaller than that calculated in power build up cavity by M. de Labachelerie et al. for the same line. Using these measured P_{sat}, these measured widths can be compared to those expected from transit time broadening.

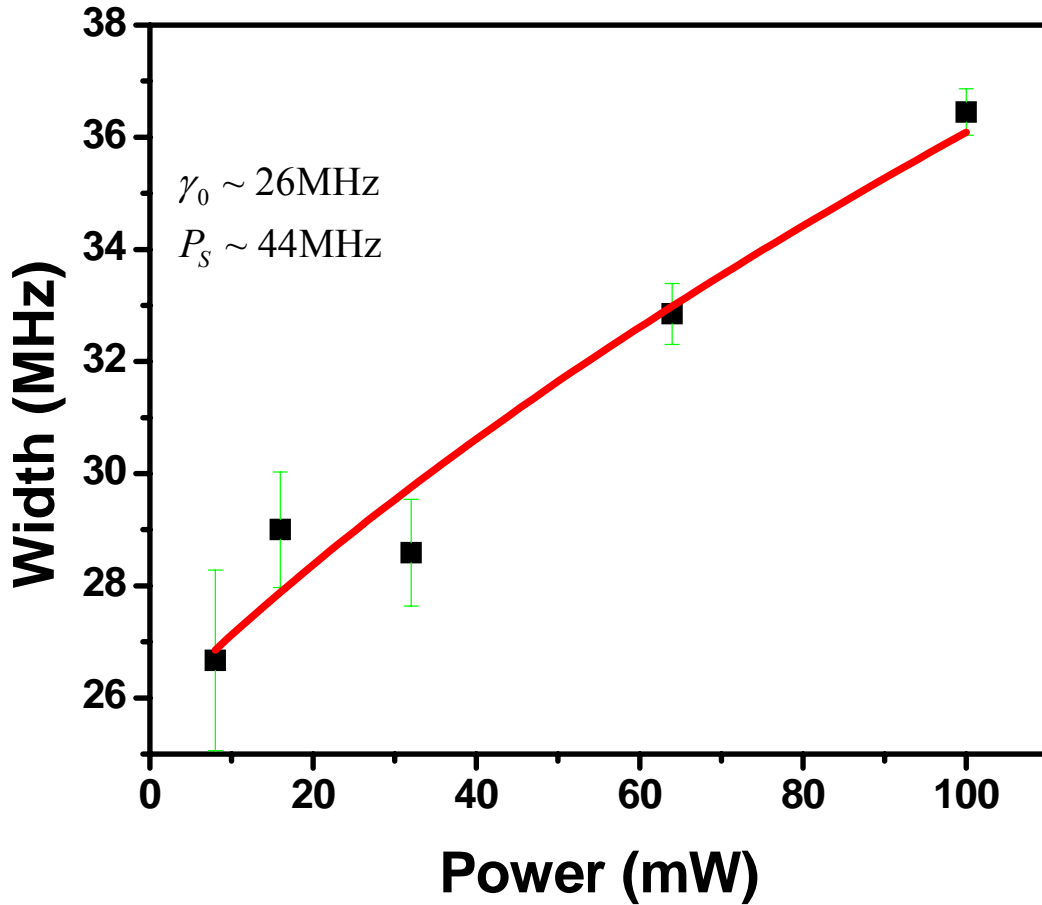Fig. 6.9. Power broadening effect on the resonance linewidth, p (11) at pressure of 1 Torr. The theoretical fit is based on the formalism explained in Eq [23].

The extrapolated zero pressure value for P (11) and P (13) lines as shown in fig. 6.7 should be compared to the expected power broadening plus transit time broadening. The calculated transit time limit, for room temperature molecules weighing 26 a.u. in a

13.5 μm diameter light field is 25 MHz. Taking a saturation power of 25-50 mW, this calculated width should broaden to be 31-37 MHz at 29 mW, and 29-32 MHz at 14 mW. These values are in general 1.5-2 times larger than the observed values. The discrepancy may be due to propagation effects along the length of fiber.

For the optimum gas pressure for laser frequency stabilization, it is necessary to use lower pressure. The reason is due to pressure broadening. Usually at high pressures, the power broadening effect is not significant. In order to remove the Doppler character completely and to obtain a flat base line, careful alignments of the beams are necessary so that polarizations of the pump beam and the counter-propagating probe beam are perpendicular to each other.

In particular, we are interested in the determination of the optimum pressure for the maximum signal slope. The maximum signal slope will have the larger signal with smaller width which in turn gives the better resolution of the peak frequency. We want to use that signal to stabilize the laser frequency. Figure 6.10 below shows the measured signal slope (filled squares) for the P (11) line. Signal slope is the ratio of the signal size in units of fractional absorption to the width, ω_l of the narrow feature. It can be written by the expression,

$$\text{Signal Slope} = \frac{\exp(-A_g(1-A_l))-\exp(-A_g)}{\omega_l(MHz)}$$

where A_g is the amplitude of the Gaussian profile and A_g times A_l is the amplitude of the narrow feature.
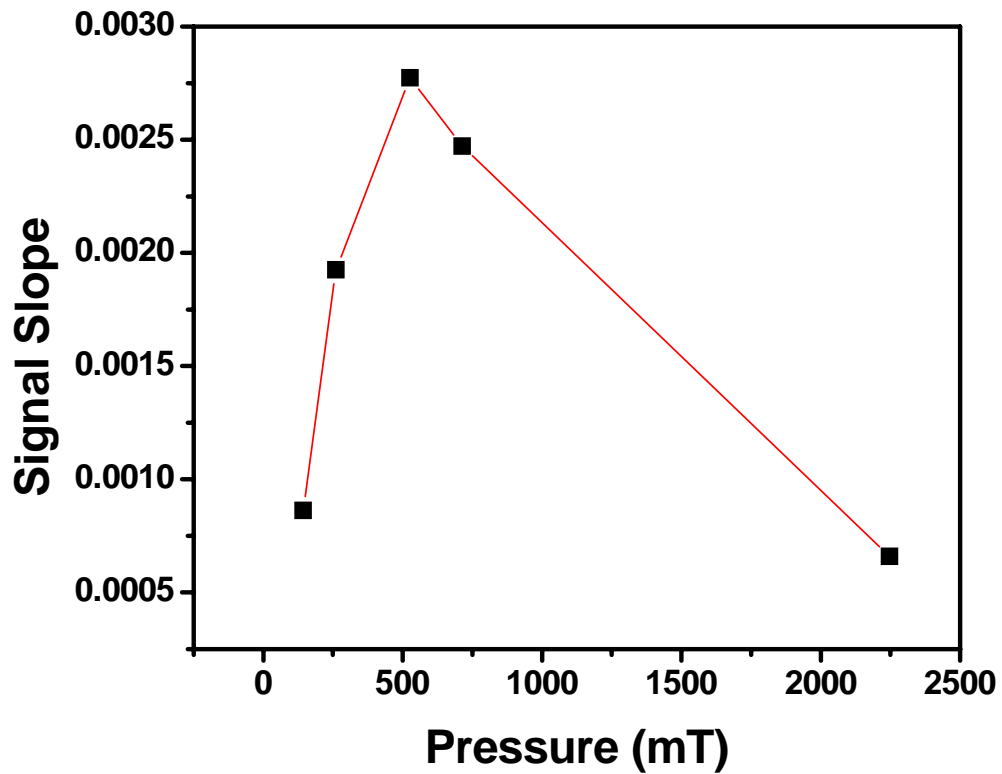
Fig. 6.10. Measured signal slope for P (11) line. Signal slope is the ratio of the signal size in units of fractional absorption to the width, ω_l of the narrow feature. A_g is the amplitude of the Gaussian profile and A_g times A_l is the amplitude of the narrow feature.

It is found that the optimum pressure for an 80 cm long, 20 μm fiber is ~530 mT when pumped with 29 mw. This is the consistent with the signal size as visually seen in Fig. 6.5. As the fiber length increases, the optimum pressure condition will further decrease. Optimum pressure conditions also depend upon the optical power.

CHAPTER 7

Conclusion and future direction

For a molecule to absorb infrared light, the vibrations or rotations within a molecule must cause a net change in the dipole moment of the molecule. The alternating electrical field of the radiation interacts with fluctuations in the dipole moment of the molecule. If the frequency of the radiation matches the vibrational frequency of the molecule then radiation will be absorbed, causing a change in the amplitude of molecular vibration.

We have carried out several experiments studying the line shapes and the way in which pressure, power and transit time broaden the resonance feature. Pressures were measured using an MKS Baratron and thermocouple gauge, calibrated in the range of 50 mT to 2500 mT with 10% error in pressure measurement. As we increase the gas pressure inside the cavity, we witness linewidth broadening. Extrapolating these curves to zero pressure should reveal a power-broadened plus transit time broadened feature. We found the extrapolated value to be 21 MHz at the power of 29 mW for the P (11) line and 17 MHz at a power of 14 mW for the P (13) line. Taking a saturation power of 25-50 mW, calculated widths range from 31-37 MHz at 29 mW and 29-32 MHz at 14 mW. The discrepancy may be due to propagation effects along length of fiber.

We have showed that the saturated absorption is readily achievable in photonic band gap fiber with power less than 10 mW. The signal-to-noise ratio (SNR) on the different transitions is significantly improved by careful alignment of the beams, by controlling suitable polarization between pump and probe beams, and by increasing the

probe power. The improved SNR makes overtone transitions in the near-infrared region accessible to frequency metrology.

We have investigated the dependence of signal quality on vapor pressure and power output from the fiber. In fact, fiber core size sets optimum pressure, power, length, and linewidth. Narrower lines require larger cores, lower pressure and longer lengths. We are on the way to further narrowing the transition by using larger core fiber or by coating the inner side of the fiber in order to maintain longer coherence time between molecules and the laser beam. We have made substantial progress toward characterization of the dependence of linewidth, line shift and signal size on pressure, power, diameter and length of the fiber. In future, we will lock a laser to the transition, and characterize the frequency stability plus shift as a function of these parameters.

Acetylene inside the PBG fiber is a promising system for a stable, high-accuracy, portable frequency standard in the near-infrared region. We are on the way toward sealing the PBG fibers on the both ends with solid core fiber, eliminating the need for the vacuum system. We also plan to measure the optical frequency of this transition using a frequency comb. Our ultimate goal is to create high-accuracy, portable optical frequency references.

References:

1.   Demtroder, W., *Laser Spectroscopy*. Third ed. 2002: Springer. 987.
2.   Delabachelerie, M., K. Nakagawa, and M. Ohtsu, *Ultranarrow (C2h2)-C-13 Saturated-Absorption Lines at 1.5 Mu-M.* Optics Letters, 1994. **19**(11): p. 840-842.
3.   Nakagawa, K., et al., *Accurate optical frequency atlas of the 1.5-mu m bands of acetylene.* Journal of the Optical Society of America B-Optical Physics, 1996. **13**(12): p. 2708-2714.
4.   Sarah L. Gilbert, W.C.S., *Acetylene $_{12}C_2H_2$ Absormtion Reference for 1510 nm to 1540 nam Wavelength Calibration-SRM 2517a.* 2001.
5.   Delabachelerie, M., et al., *High-Frequency-Stability Laser at 1.5 Mu-M Using Doppler-Free Molecular Lines.* Optics Letters, 1995. **20**(6): p. 572-574.
6.   Swann, W.C. and S.L. Gilbert, *Pressure-induced shift and broadening of 1510-1540-nm acetylene wavelength calibration lines.* Journal of the Optical Society of America B-Optical Physics, 2000. **17**(7): p. 1263-1270.
7.   Washburn, B.R., et al., *Fiber-laser-based frequency comb with a tunable repetition rate.* Optics Express, 2004. **12**(20): p. 4999-5004.
8.   Corwin, K.L., et al., *Absolute-frequency measurements with a stabilized near-infrared optical frequency comb from a Cr: forsterite laser.* Optics Letters, 2004. **29**(4): p. 397-399.
9.   Hong, F.L., et al., *Absolute frequency measurement of an acetylene-stabilized laser at 1542 nm.* Optics Letters, 2003. **28**(23): p. 2324-2326.
10.   Czajkowski, A., et al., *Absolute frequency measurement of acetylene transitions in the region of 1540 nm.* Applied Physics B-Lasers and Optics, 2004. **79**(1): p. 45-50.
11.   Edwards, C.S., et al., *Absolute frequency measurement of a 1.5-mu m acetylene standard by use of a combined frequency chain and femtosecond comb.* Optics Letters, 2004. **29**(6): p. 566-568.
12.   Knight, j.C., *Photonic crystal fibers.* nature, 2003. **424**: p. 847.
13.   Knight, J.C., et al., *All-silica single-mode optical fiber with photonic crystal cladding: Errata.* Optics Letters, 1997. **22**(7): p. 484-485.
14.   Ritari, T., et al., *Gas sensing using air-guiding photonic bandgap fibers.* Optics Express, 2004. **12**(17): p. 4080-4087.
15.   Benabid, F., et al., *Ultrahigh efficiency laser wavelength conversion in a gas-filled hollow core photonic crystal fiber by pure stimulated rotational Raman scattering in molecular hydrogen.* Physical Review Letters, 2004. **93**(12).
16.   *Advanced Chemical Experimentation and Instrumentation,MIT http://web.mit.edu/5.33/www/Exp1_IR_05.pdf.* 2005.
17.   Birks, T.A., J.C. Knight, and P.S. Russell, *Endlessly single-mode photonic crystal fiber.* Optics Letters, 1997. **22**(13): p. 961-963.
18.   Zheltikov, A.M., *Holey fibers.* Uspekhi Fizicheskikh Nauk, 2000. **170**(11): p. 1203-1215.
19.   Tseng, I.-C., *http://ethesys.lib.fcu.edu.tw/ETD-db/ETD-search/view_etd?URN=etd-0730103-145939.* 2002.
20.   Benabid, F., et al., *Compact, stable and efficient all-fibre gas cells using hollow-core photonic crystal fibres.* Nature, 2005. **434**(7032): p. 488-491.